RESEARCH ARTICLE

Mapping Synaptic Cortico-Claustral Connectivity in the Mouse

Gal Atlan,[1] Anna Terem,[2] Noa Peretz-Rivlin,[1] Maya Groysman,[1] and Ami Citri[1,2]*

[1]Edmond and Lily Safra Center for Brain Sciences, Jerusalem, Israel
[2]Department of Biological Chemistry, Institute of Life Sciences, Hebrew University of Jerusalem, Edmond J. Safra Campus, Givat Ram, Jerusalem, Israel

The claustrum is an intriguing brain structure, featuring the highest connectivity per regional volume in the brain. It is a thin and elongated structure enclosed between the striatum and the insular cortex, with widespread reciprocal connections with the sensory modalities and prefrontal cortices. Retinotopic and somatotopic organizations have been described in the claustrum, and anatomical studies in cats, monkeys, and rats have demonstrated topographic organization of cortico-claustral connections. In this study we mapped the projections from cortical modalities (visual, auditory, somatosensory, motor, and olfactory), and prefrontal regions (anterior cingulate cortex and orbitofrontal cortex) to the claustrum in mice. Utilizing expression of a virally encoded synaptic anterograde tracer, AAV-SynaptoTag, followed by 3D reconstruction of the cortical projections, we performed a comprehensive study of the organization of these projections within the mouse claustrum. Our results clearly demonstrate a dorsoventral laminar organization of projections from the sensory cortices to the claustrum, whereas frontal inputs are more extensive and overlap with the inputs from the sensory cortices. In addition, we find evidence supporting a core/shell organization of the claustrum. We propose that the overlap between the frontal inputs and the inputs from the sensory modalities may underlie executive regulation of the communication between the claustrum and the cortical modalities. J. Comp. Neurol. 000:000–000, 2016.

INDEXING TERMS: anterograde tracing; sensory modalities; association cortices; dorsoventral organization; RRID: AB_221570

The claustrum, a thin elongated sheet of neurons located between the insular cortex and the striatum, is the most interconnected structure in the brain per regional volume (Torgerson et al., 2015). The claustrum has been reported to display prominent reciprocal connectivity with essentially the entire cerebral cortex (Narkiewicz, 1964; Riche and Lanoir, 1978; Sanides and Buchholtz, 1979; Olson and Graybiel, 1980; LeVay and Sherk, 1981a,b; Macchi et al., 1981, 1983; Sherk and LeVay, 1981a,b, 1983; Pearson et al., 1982; Carey and Neal, 1985, 1986; LeVay, 1986; Sloniewski et al., 1986; Grieve and Sillito, 1995; Sadowski et al., 1997; Beneyto and Prieto, 2001; Tanne-Gariepy et al., 2002; Alloway et al., 2009; Smith and Alloway, 2010, 2014; Park et al., 2012; Smith et al., 2012; Druga, 2014; Milardi et al., 2015). The broad cortical connections of the claustrum suggest it might serve as a network hub, coordinating activity of the cortical circuitry (Zingg et al., 2014). However, the anatomical structure of the claustrum is restrictive for functional perturbations, leaving the function of the claustrum a mystery.

Excitation of the different sensory modalities elicits responses in claustral neurons, which typically exhibit a low firing rate in the absence of stimuli (Segundo and Machne, 1956; Olson and Graybiel, 1980; Sherk and LeVay, 1981b; Remedios et al., 2010). While some studies have described multimodal responses in the claustrum (Segundo and Machne, 1956; Spector et al., 1974; Clarey and Irvine, 1986), other studies (Olson and Graybiel, 1980; Sherk and LeVay, 1981b; Remedios et al., 2010) failed to find multimodal cells in the claustrum, but rather found clear-cut regional specialization.

Grant sponsor: Adelis Foundation Brain Research Award; Grant sponsor: National Institute for Psychobiology in Israel, Founded by the Charles E. Smith Family (109-15-16).

*CORRESPONDENCE TO: Ami Citri, Room 2-516, Silberman Building, Safra Campus of the Hebrew University, Givat Ram, Jerusalem 91904, Israel. E-mail: ami.citri@mail.huji.ac.il

Received November 1, 2015; Revised February 27, 2016;
Accepted March 4, 2016.
DOI 10.1002/cne.23997
Published online Month 00, 2016 in Wiley Online Library (wileyonlinelibrary.com)

This leaves open the issue of whether claustral neurons integrate or segregate sensory information, a crucial issue for understanding the function of the claustrum.

The responses of claustral neurons to visual stimulation display a retinotopic organization in cats (Olson and Graybiel, 1980; LeVay and Sherk, 1981b; Sherk and LeVay, 1981b). Similarly, auditory-responsive claustral neurons in both cats and primates have been found to be loosely tuned and display broad receptive fields, responding preferentially to the onset of a stimulus (Olson and Graybiel, 1980; Clarey and Irvine, 1986; Neal et al., 1986; Beneyto and Prieto, 2001; Remedios et al., 2010, 2014). Somatosensory responses have also been reported in the claustrum of cats, with reports of somatotopic organization (Spector et al., 1970, 1974; Olson and Graybiel, 1980).

Numerous studies in the past half-century have addressed the organization of inputs into the claustrum of monkeys, cats, rabbits, and rats (Sanides and Buchholtz, 1979; LeVay and Sherk, 1981b; Sherk and LeVay, 1981b; Witter et al., 1988; Kowianski et al., 1998; Mathur, 2014). The anatomy corresponds well with the physiological studies, such that different cortical inputs map to segregated domains within the claustrum. Thus, both rostrocaudal and dorsoventral segregation have been proposed for the claustrum, albeit with a high degree of overlap. The claustrum also displays asymmetric reciprocal connectivity with the cortex, such that a given cortical modality receives input not only from its corresponding sensory zone in the claustrum, but from adjacent claustral regions as well. This asymmetry suggests that a given sensory zone in the claustrum may exert influence on additional cortical regions beyond those which innervate it (Narkiewicz, 1964; Norita, 1977; Riche and Lanoir, 1978; Olson and Graybiel, 1980; LeVay and Sherk, 1981b; Macchi et al., 1981, 1983; Sherk and LeVay, 1981b; Pearson et al., 1982; Carey and Neal, 1985; Minciacchi et al., 1985; Carey and Neal, 1986; Li et al., 1986; Sloniewski et al., 1986; Sadowski et al., 1997; Beneyto and Prieto, 2001; Tanne-Gariepy et al., 2002; Alloway et al., 2009; Smith and Alloway, 2010; Park et al., 2012; Zingg et al., 2014; Milardi et al., 2015).

The dorsoventral axis appears to be the prominent axis along which inputs are organized in the rat, rabbit, cat, and primate (Olson and Graybiel, 1980; Sadowski et al., 1997; Kowianski et al., 1998; Remedios et al., 2010). The ventral region of the primate claustrum has been associated with vision and the central region of the claustrum with audition. In the cat, the dorsoventral axis also appears dominant, but a reversed spatial order is found, such that the visual claustrum of the cat is found in the dorsal section of the claustrum, receiving convergent input from several ipsilateral visual cortical areas, and projecting back to these same areas (Sanides and Buchholtz, 1979; LeVay and Sherk, 1981a,b; LeVay, 1986; Smith and Alloway, 2014). Inputs from auditory cortex to the cat claustrum concentrate in the center of the dorsoventral axis, throughout the rostrocaudal axis, and are primarily ipsilateral. Interestingly, the auditory region in the cat claustrum appears to receive inputs from several distinct auditory cortical regions (Neal et al., 1986; Beneyto and Prieto, 2001). Somatosensory inputs have been described in the dorsal part of the cat and primate claustrum, as have somatomotor inputs in rats and mice (Olson and Graybiel, 1980; Sadowski et al., 1997; Kunzle and Radtke-Schuller, 2001; Smith et al., 2012; Smith and Alloway, 2014; Zingg et al., 2014). In contrast to the segregation described for inputs from the sensory modalities within the claustrum, inputs from the prefrontal cortex and anterior cingulate cortex have been found to extend along the dorsoventral axis of the claustrum (LeVay and Sherk, 1981b; Reser et al., 2014; Sherk, 2014). The output from the claustrum to the cortex has also been demonstrated to portray a dorsoventral organization in the rat (Sadowski et al., 1997), with a dorsal sensorimotor zone and a ventral visuoauditory zone. In contrast, a recent study in rats found that claustral neurons projecting to different sensory cortices localized to discrete zones, but a topographical organization could not be discerned (White et al., 2016).

The mouse is the leading animal model for the majority of contemporary neurophysiological and behavioral studies. Albeit the availability of multiple resources for gene expression and connectivity mapping (e.g. the Allen Brain Atlas, http://mouse.brain-map.org; Mouse Connectome Project http://www.mouseconnectome.org; Waxholm Space Atlas), the mouse has been almost completely neglected in terms of investigation of claustral anatomy, with only two studies published in which projections to the claustrum have been considered (Zingg et al., 2014; Smith and Alloway, 2014). With the reinvigoration of excitement around the claustrum (Crick and Koch, 2005; Mathur, 2014; Goll et al., 2015), it has become urgent to map the cortical inputs to the claustrum in the mouse, in anticipation of functional studies applying the variety of molecular tools available for neurophysiological research in mice.

In this study we set out to map the projections from cortical modalities and association regions onto the claustrum of the mouse. Applying a molecular strategy to anterogradely label presynaptic terminals from defined cortical projections to the mouse claustrum, followed by 3D reconstruction of the cortical projections, we provide a comprehensive and detailed view of the organization of these projections in the claustrum of the mouse.

TABLE 1.
Injection Sites for All Mice

Mouse #	Stereotaxic coordinates of injection center (LM, RC, DV)	Injected SynaptoTag volume (nl)
OI#1	0.5,+2.8,−3.75	50
OI#2	1.6, +2.8,−3.75	50
Fr#1	0.25,+1.1,−1.75	350
Fr#2	0.25,+1.1,−1.75	100
Fr#3	1, 2.55,−2.4	200
Fr#4	1, 2.55,−2.4	200
Fr#5	1, 2.55,−2.4	200
Sm#1	1.8, +1.33,−1.5	300
Sm#2	1.8, +1.33,−1.5	300
Sm#3	3.2,−0.5,−1.7	300
Au#1	4,−2.8,−2.6	300
Au#2	3.8,−2.46,−2.3	100
Au#3	4,−2.3,−2.75	100
Au#4	3.8,−2.7,−1.8	250
Vi#1	2.25, −3.4,−1.1	300
Vi#2	2.25, −3.4,−1.1	300
Vi#3	3.25,−3.64,−1.8	200
PV-Cre;Ai9 Au	4,−2.8,−2.6	300
PV-Cre;Ai9 Fr	1, 2.55,−2.4	200

MATERIALS AND METHODS

Animals

The mice used for connectivity analysis were female wildtype C57BL6 mice aged 6–8 weeks (n = 17). PV-CRE;Ai9 mice (12-week-old females; n = 2) were used to address the core/shell organization of the claustrum. PV-CRE;Ai9 are PV-CRE knock-in mice crossed to the Ai9 line for conditional (CRE-dependent) expression of tdTomato (Madisen et al., 2010) and were kindly provided by Prof. Adi Mizrahi. Mice were kept on a 12-hour light-dark cycle in a specific pathogen-free (SPF) animal facility with free access to food and water. All experimental procedures, handling, surgeries, and care of laboratory animals used in this study were approved by the Hebrew University Animal Care and Use Committee.

AAV viral vector

An AAV viral construct encoding mCherry-IRES-eGFP-Syb2 under the regulation of the synapsin promoter was used to label the cytoplasm of presynaptic neurons (in red) as well as target an enhanced green fluorescent protein (eGFP) to synapses via its fusion to the synaptic vesicle protein, Synaptobrevin 2/VAMP2. This construct, a gift from Dr. Wei Xu (UT Southwestern Medical Center) has been previously described (Xu and Sudhof, 2013).

AAV production

AAV viruses were packaged into the AAV-DJ capsid for high efficiency in vivo neuronal infection (Xu et al., 2012; Xu and Sudhof, 2013) in the virus core facility at the Edmond and Lily Safra Center for Brain Sciences. Briefly, AAV vectors were generated by linear polyethylenimine (PEI)-mediated triple transfection of AAV transfer vector, RC-DJ, and adenovirus helper plasmids into HEK 293T cells. Seventy-two hours posttransfection, both cells and culture supernatants were separately harvested. In order to release the AAV vectors, the cells were subjected to three successive freeze–thaw cycles, then treated by benzonase and sodium deoxycolate at 37°C for 1 hour and precleared by centrifugation. The clarified cell lysates were pooled together with previously collected culture supernatants and AAV vectors were precipitated from the combined fractions by 40% PEG/2.5M NaCl incubation at 4°C for 2 hours with occasional agitation. The precipitated virus pellet was resuspended into HEPES buffer at 4°C overnight and further purified by affinity chromatography, using HiTrap Heparin HP columns (GE Healthcare, Milwaukee, WI) and finally desalted and concentrated by ultrafiltration, using Amicon Ultra-15 centrifugal filter units (Millipore, Bedford, MA).

Stereotactic surgery and virus injections

Mice were anesthetized by IP injection of ketamine (75 mg/kg) and medetomidine (1 mg/kg), and then secured in a stereotaxic apparatus (David Kopf Instruments, Tujunga, CA). Following incision of the scalp, a small hole was made in the skull using a fine drill burr (model 78001, RWD Life Science, San Diego, CA) and a microsyringe (33GA Hamilton syringe, Reno, NV) loaded with the virus was lowered into the intended brain region. The viral tracer was injected unilaterally at 50–100 nl/min via a UltraMicroPump (World Precision Instruments, Sarasota, FL), following which the microsyringe was left in the tissue for 5–10 minutes after the termination of the injection before being slowly retracted. Finally, the incision was glued with bioadhesive and the animals were injected with saline (for hydration), antisedan (to negate the anesthesia), and rimadyl (analgesia) and recovered with gentle heating. Coordinates for stereotactic injection were based on the Paxinos and Franklin (2013) mouse brain atlas, and are defined in Table 1.

Histology and immunohistochemistry

Mice were sacrificed 4–8 weeks after surgery by anesthesia with 5% isoflurane, followed by rapid decapitation. Brains were removed and fixed in 4% paraformaldehyde (PFA) overnight at 4°C. On the following day, brains were thoroughly rinsed in a 0.9% NaCl phosphate-buffered saline (PBS) solution and sectioned on a Vibratome (7000 smz-2) at 60 μM thickness in the coronal plane. Two series of sections were collected from each brain, resulting in two copies of brain slices at 120 μm apart, corresponding to the

TABLE 2.
Primary Antibody used in the Experiment

Antigen	Description of immunogen	Source, host species, Cat. #, RRID	Concentration used
GFP	GFP isolated from *Aequorea victoria*	Life Technologies, Rabbit polyclonal, # A-6455, AB_221570	1:500 dilution

division of the mouse brain atlas (Pollak Dorocic et al., 2014).

In order to enhance the eGFP signal, floating section immunohistochemistry was performed. Sectioned brain slices were washed twice in PBS, followed by blocking in 3% normal horse serum and 0.3% Triton X-100 in PBS for 1 hour. Sections were then incubated overnight at 4°C in a rabbit anti-GFP primary antibody (Life Technologies, Bethesda, MD; catalog No. A-6455; final dilution to 1:500 in 3% normal horse serum, see Table 2). Sixteen hours later the sections were washed three times in PBS. Washes were followed by 2 hours of incubation at room temperature with donkey antirabbit IgG H&L Alexa Fluor 488 (Abcam, Cambridge, UK; catalog No. Ab150065; final dilution 1:500) in 3% normal horse serum. Finally, the sections were washed three times in PBS and then counterstained with 4′,6-diamidino-2-phenylindole (DAPI; Roche, Nutley, NJ; Cat. No. 10-236-276; final dilution 1:1,000 in PBS) to detect cell nuclei and then quickly washed twice, mounted onto slides, and covered. Special care was taken to mount sections in the order they were sectioned, thereby providing context for the anatomical location of each slice along the anterior–posterior axis.

Image acquisition

Slides were scanned on a high-speed fully motorized multichannel light microscope (Olympus IX-81) in the microscopy unit of the Alexander Silberman Institute of Life Sciences. Virus injection sites were photographed at 4× magnification in the red channel (NA = 0.16; excitation 555 ± 25 nm, emission 605 ± 52 nm) in order to document mCherry expression. Exposure times were kept constant within each brain series and were selected so that single infected cells at the center of the injection site would be readily discernable. Brain slices containing the claustrum were imaged at 10× magnification (NA = 0.3; excitation 490 ± 20 nm, emission 525 ± 36) using low gain. Green channel exposure times were selected such that the fluorescent signal in the region of the claustrum would provide single puncta resolution, potentially corresponding to individual synapses. Settings were kept constant within each brain series. Corresponding DAPI images were acquired using excitation filters of 350 ± 50 nm, emission 455 ± 50 nm.

Image digitization and analysis

In order to create a 3D reconstruction of the mouse brain, we constructed a stack of 96 binary images from the 96 corresponding plates in the Paxinos and Franklin mouse brain atlas (2013) (figures 25, 32, 39 of the atlas were excluded).

Individual brain slices containing the claustrum were matched to the appropriate section in the atlas using nearby anatomical markers (landmarks included the location and orientation of the external capsule and anterior commissure, the size and orientation of the ventricles, and the shape and orientation of the piriform cortex) as well as more nuanced cues obtained from the size, density, and orientation of DAPI-stained nuclei and the annotation of adjacent (preceding and proceeding) sections. This methodology of matching of slices to the atlas with multiple references, including consistent matching across slices to maintain a reference in the rostral-caudal axis, was also helpful in correcting for tilts that occur in the plane of sectioning. In almost all cases, the anatomical definition of the claustrum was verified by at least two independent investigators. The anatomical boundaries of the claustrum were then overlaid onto the fluorescent image and the spread of infected cells and labeled projections was digitized using a 3 × 3 pixel sized brush (corresponding to ∼22 microns). This provided a binary representation in 3D space of the injection site and the location of projections in the claustrum. A similar stack, in which the contour of the claustrum was completely filled in, was used to represent the form of the claustrum (Fig. 1). Digitization and stack creation was performed using ImageJ (NIH open source, Bethesda, MD). Digitized stacks were converted into 3D objects using Imaris (v. 7.6.5. Bitplane, Zurich, Switzerland), and were overlaid to create projection maps (Fig. 1). It is important to note that our method of analysis focused solely on the anatomical spread of cortical terminals in the claustrum, and thus, the intensity of the signal, as well as fine details of the synaptic organization, were not represented in the digitization.

Figures were prepared using Photoshop, Illustrator, and InDesign (Adobe CS6, San Jose, CA). Figures showing stained brain tissue were adjusted using a uniform brightness/contrast mask created in linear-mode in Photoshop, and applied consistently to all slices within

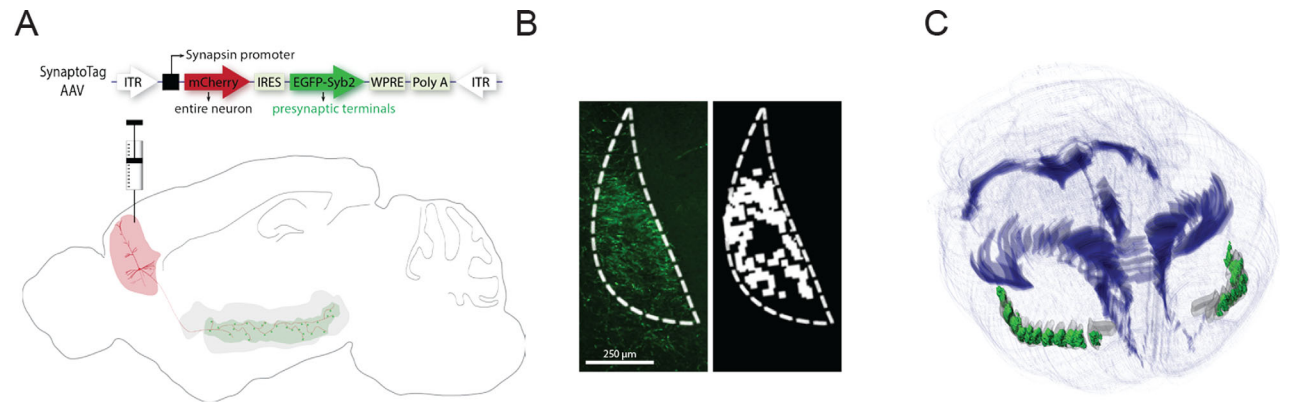

Figure 1. Experimental strategy for mapping cortical projections to the claustrum. (**A**) Top: scheme of the AAV-SynaptoTag vector for anterograde tracing. Neurons infected with AAV-SynaptoTag express mCherry throughout the cell, while their efferent presynaptic boutons are labeled with eGFP, due to the fusion to the synaptic vesicle protein Synaptobrevin2/VAMP2 (Syb2). Bottom: illustration of the cortical injection site expressing cytoplasmic red fluorescence, as well as presynaptic terminals in the claustrum labeled in green fluorescence, defining an innervated subregion within the claustrum. (**B**) Digitization method. Left: high-magnification image of the claustrum demonstrating projections from the auditory cortex following immunohistochemistry to enhance the eGFP signal. The dotted line represents the outline of the claustrum as defined in the corresponding panel from the Paxinos and Franklin brain atlas. Right: binary image following digitization of the signal corresponding to the projections within the claustrum. (**C**) Example of the 3D reconstruction of the mouse brain and claustrum, with projections from auditory cortex (green). Reconstructed models were built from overlaying three separate binary image stacks: one consisting of the atlas panels with no signal (blue outline), one of the entire claustrum (gray), and one of the digitized signal of the projections to the claustrum (green).

a single brain. For presentation, in cases where a slice was unusually uniformly dark compared to its neighboring slices, separate adjustments of brightness/contrast were performed in order to achieve a consistent level of base fluorescence within each figure. Images were then scaled or cropped. In one case (Vi#1), dust speckles were digitally removed from the image in Photoshop. All digitization was performed on raw, nonadjusted images.

RESULTS

3D reconstruction of cortical synaptic inputs to the claustrum

To study the organization of cortical synaptic inputs within the claustrum, we made use of an AAV virus expressing a bicistronic cassette under the control of the synapsin promoter ("SynaptoTag"). The SynaptoTag vector expresses a soluble red fluorescent protein (mCherry) to label infected neurons and their processes, as well as an enhanced green fluorescent protein fused to the synaptic vesicle protein VAMP2/synaptobrevin-2 (eGFP-Syb2)—labeling synaptic terminals of these neurons at their projection sites (Xu and Sudhof, 2013). Synaptic terminals were visible when they converged in a defined anatomical location, such as the claustrum. However, as the virus expresses eGFP as a fusion construct of Syb2, in a bicistronic cassette, the strength of the eGFP signal is limited. Antibody staining against eGFP provided specific amplification of the signal, resulting in clear and prominent labeling of terminals within the claustrum. This approach, combined with DAPI staining, allowed the use of anatomical markers to match brain slices to specific plates in the mouse brain atlas. Digitizing this signal enabled registration of the coordinates of the synaptic input to the claustrum from each cortical site, from which a 3D reconstruction was compiled. Overlaying these 3D reconstructions enabled investigation of the relative location and spread of each cortical input to the claustrum (Fig. 1).

In order to map the cortical inputs to the claustrum, 17 mice were injected with the AAV-SynaptoTag virus in five different classes of cortical regions: visual (Vi#1-3), auditory (Au#1-4), somatomotor (Sm#1-3), olfactory (Ol#1-2), and prefrontal (Fr#1-5) (see Table 1 for injection coordinates and volumes). Two additional mice, of the PV-Cre; Ai9 strain, underwent injections to auditory or prefrontal cortex in order to study the spread of these inputs in relation to the PV-rich core of the claustrum. The vast majority of labeled cells were located in cortical layer 5, as well as layers 2/3. Our analysis focused on the anatomical spread of labeled synapses in the claustrum. We describe the organization of inputs to the claustrum from the sensory cortices and prefrontal regions in mice, and discuss the organizational principles emerging from this study.

Visual inputs to the claustrum

We studied the inputs from visual areas to the claustrum in three mice (Fig. 2). Two injections, in mice Vi#1

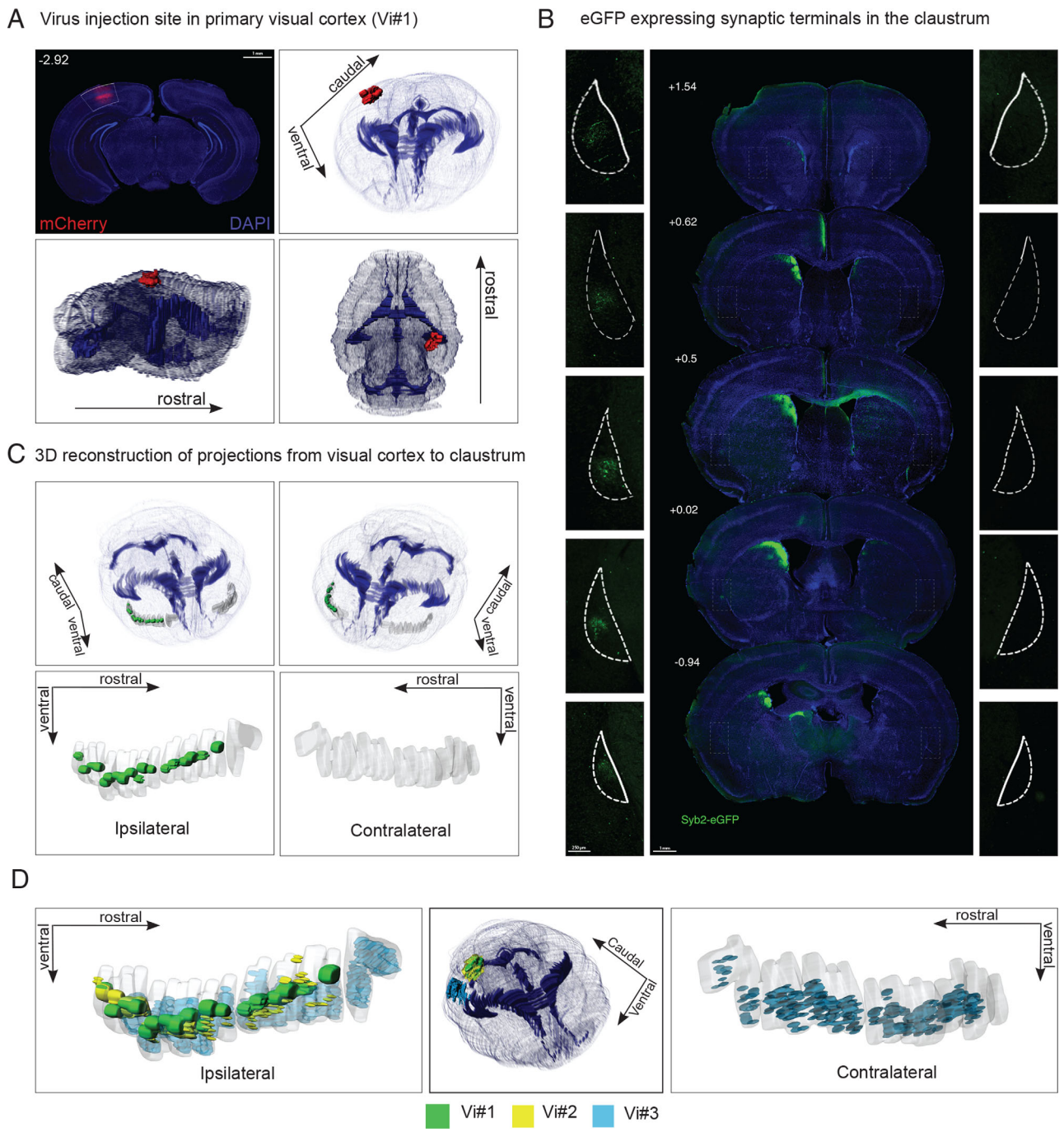

Figure 2. Projections from the visual cortex to the claustrum. (**A**) Top left: coronal section corresponding to the AAV-SynaptoTag injection site in the primary visual cortex of mouse Vi#1; DAPI nuclear staining in blue; mCherry expression in red. Number indicates distance in mm from Bregma. Bottom left: reconstructed 3D view of the spread of the infection, as seen from the side. Bottom right: injection site as seen from above. Top right: angular view of the injection site. (**B**) Representative brain sections in rostrocaudal order. Middle: whole section images of visual cortical projections following immunostaining against eGFP. Numbers indicate distance from Bregma in mm. Side panels: ipsilateral (left) and contralateral (right) claustrum. (**C**) 3D reconstruction of the target region in the claustrum. Top left and right panels: angular view of the whole brain and overlay of the ipsilateral claustrum and contralateral claustrum, respectively. Bottom left: reconstructed fluorescent signal in the ipsilateral claustrum. Bottom right: reconstructed fluorescent signal in the contralateral claustrum. The gray background is the outline of the reconstructed claustrum. (**D**) 3D superposition of all mice injected with AAV-SynaptoTag to the visual cortex (Vi#1, Vi#2, Vi#3). Different color hues refer to individual mice according to the legend, enabling a comparison of individual injections and their projection to the claustrum. Left: reconstruction of the innervated region in the ipsilateral claustrum. Middle: angular view of the spread of each infection in the site of origin. Right: reconstruction of the innervated region in the contralateral claustrum.

and Vi#2, were to the rostral primary visual cortex. Infected cells were entirely localized to the primary visual cortex, with a broader domain of infection in mouse Vi#1 than in mouse Vi#2. Mouse Vi#3 was injected in the lateral area of the secondary visual cortex. The rostral part of the infection site in this case included a small number of labeled cells in the dorsal secondary auditory cortex. In accordance with previously published data, visual inputs were found in the dorsomedial striatum and the anterior cingulate cortex (Khibnik et al., 2014; Reig and Silberberg, 2014; Zingg et al., 2014).

Primary visual inputs, observed in the claustrum of mice Vi#1 and Vi#2, were relatively sparse, exclusively ipsilateral, extended across the rostrocaudal axis, and were focused within the middle third of the claustrum in its dorsoventral axis. In contrast to the sparse signal observed in mice Vi#1 and Vi#2, dense ipsilateral signals were observed in mouse Vi#3, whose injection was primarily within the secondary visual area. The innervation from the secondary visual cortex was also more widespread than that arising from primary visual inputs, and extended to the ventral half of the claustrum, as well as labeling the contralateral claustrum (Fig. 2).

Auditory inputs to the claustrum

We studied the auditory inputs to the claustrum in four mice (Fig. 3). In two of the mice (Au#1, Au#2) the infected cells were found within A1 (primary auditory cortex) and AuD (secondary auditory cortex dorsal), with the region infected in mouse Au#2 comprising a smaller population of neurons. In mouse Au#3, we observed infected cells in A1 and AuV (ventral secondary auditory cortex). In mouse Au#4 the infection was confined to the dorsal field of the secondary auditory cortex.

In all mice, labeled terminals were found in the medial striatum, a major target of the auditory cortex (McGeorge and Faull, 1989), as well as in medial orbitofrontal cortex (data not shown) (Zingg et al., 2014). Inputs from auditory cortex to the claustrum were primarily ipsilateral, such that in mouse Au#4, which was infected in the dorsal secondary auditory area, the fluorescent signal was detected only in the ipsilateral claustrum, while in mice Au#1 and Au#3 some contralateral signal was observed, but it was much less prominent than the ipsilateral projection (mouse Au#2 had a relatively small number of infected cells and no contralateral fluorescence was observed). The signal in the ipsilateral claustrum extended the entirety of its rostrocaudal axis in all four mice. In the dorsocaudal axis it covered the central and ventral portions of the claustrum, excluding its dorsal third.

Somatomotor inputs to the claustrum:

We compared inputs from primary motor cortex and primary somatosensory cortex to the claustrum in three mice. Two of the injections, in mice Sm#1 and Sm#2, were to the motor cortex and one was to the somatosensory cortex (Figs. 4–6).

Motor cortex

In mouse Sm#1, infected cells were spread throughout a large part of primary motor cortex, with a few cells infected in M2, while in mouse Sm#2 a smaller number of neurons were infected, centered in M1. In both cases, fluorescent signals were found across the striatum and the thalamus, as well as in the contralateral M1, compatible with previous reports (Beier et al., 2013; Zhou et al., 2013). In both mice, eGFP-labeled inputs to the claustrum were localized to its dorsal tip. Fluorescently labeled terminals were relatively sparse and almost exclusively contralateral to the injection site, appearing to emerge from the corpus callosum and invading the claustrum from its dorsal aspect (Fig. 4).

Somatosensory cortex

A single mouse, Sm#3, was injected in the primary somatosensory cortex. In accordance with previously published data, fluorescent signals indicating somatosensory inputs were found in contralateral S1, the dorsolateral striatum, and primary motor cortex (Zhou et al., 2013; Khibnik et al., 2014; Reig and Silberberg, 2014; Petrof et al., 2015). Fluorescent signals were found bilaterally in the dorsal aspect of the claustrum, albeit more prominent on the ipsilateral side. Interestingly, this feature is graded along the rostrocaudal axis: while in the rostral part of the claustrum the signal is exclusively ipsilateral, in its caudal part the signal becomes bilateral, although still more prominent on the ipsilateral side (Fig. 5).

Overlaying the inputs to the claustrum from motor cortex and somatosensory cortex, it is clear that these inputs overlap in the dorsal most part of the claustrum. Yet the somatosensory inputs are mainly ipsilateral, while the motor inputs are more prominent contralaterally (Fig. 6).

Olfactory projections to the claustrum

We studied olfactory input to the mouse claustrum in two mice (Ol#1 and Ol#2; Fig. 7). The injection in mouse Ol#1 infected the caudal end of the olfactory bulb. Infected cells were spread throughout the medial olfactory bulb and the medial anterior olfactory cortex (Fig. 7). A small fraction of infected cells were located

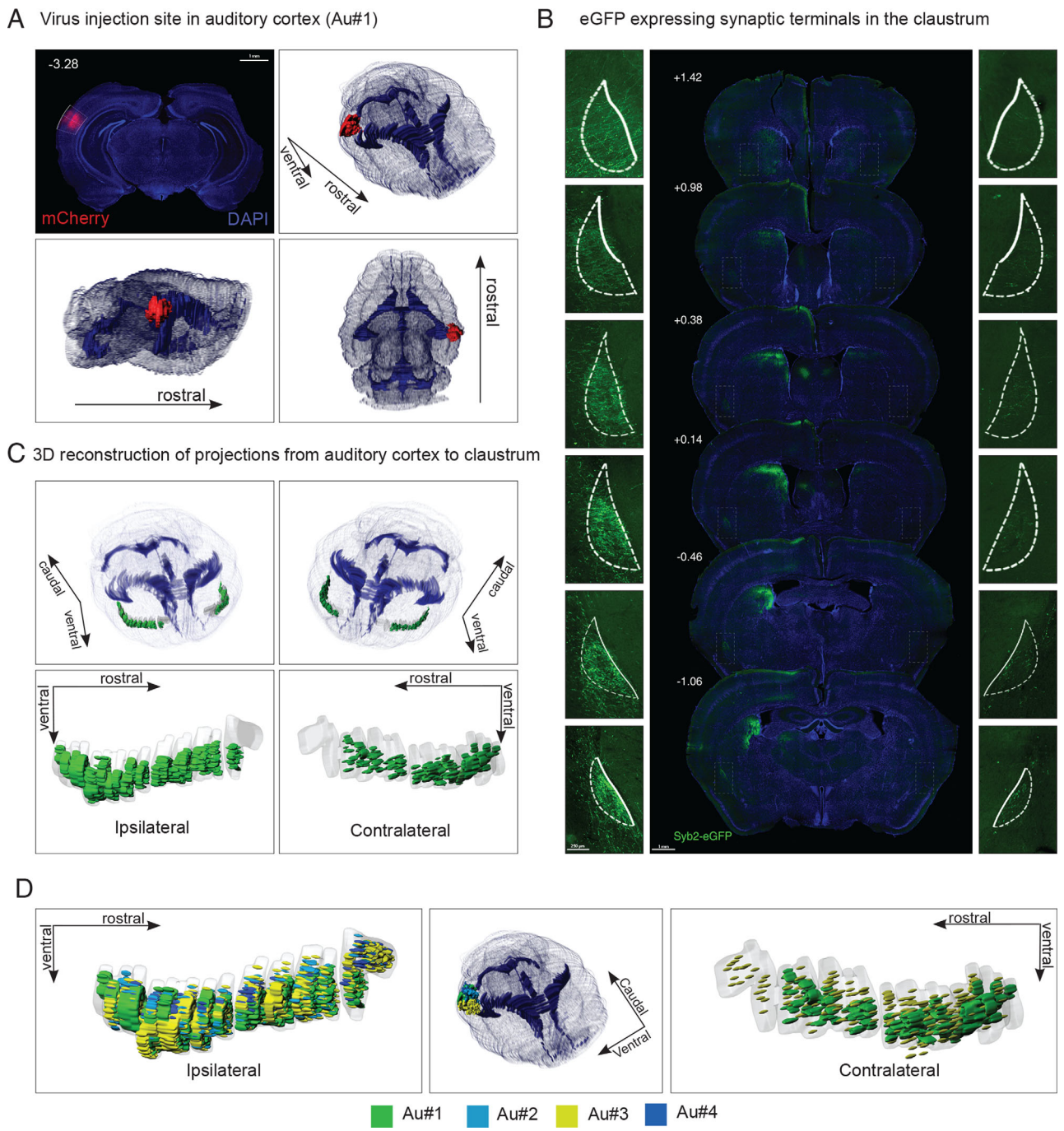

Figure 3. Projections from the auditory cortex to the claustrum. (**A**) Top left: coronal section corresponding to the AAV-SynaptoTag injection site in the primary auditory cortex of mouse Au#1; DAPI nuclear staining is shown in blue; mCherry expression in red. Number indicates distance from Bregma in mm. Bottom left: reconstructed 3D view of the spread of the infection, as seen from the side. Bottom right: injection site as seen from above. Top right: angular view of the injection site. (**B**) Representative brain sections in rostrocaudal order. Middle: whole section images of auditory cortical projections following immunostaining against eGFP. Numbers indicate distance from Bregma in mm. Side panels: ipsilateral (left) and contralateral (right) claustrum. (**C**) 3D reconstruction of the target region in the claustrum. Top left and right panels: angular view of the whole brain and overlay of the ipsilateral claustrum and contralateral claustrum, respectively. Bottom left: reconstructed fluorescent signal in the ipsilateral claustrum. Bottom right: reconstructed fluorescent signal in the contralateral claustrum. The gray background is the outline of the reconstructed claustrum. (**D**) 3D superposition of all mice injected with AAV-SynaptoTag in the auditory cortex (Au#1, Au#2, Au#3, Au#4). Different color hues refer to individual mice according to the legend, enabling a comparison of individual injections and their projection to the claustrum. Left: reconstruction of the innervated region in the ipsilateral claustrum. Middle: angular view of the spread of each infection in the site of origin. Right: reconstruction of the innervated region in the contralateral claustrum.

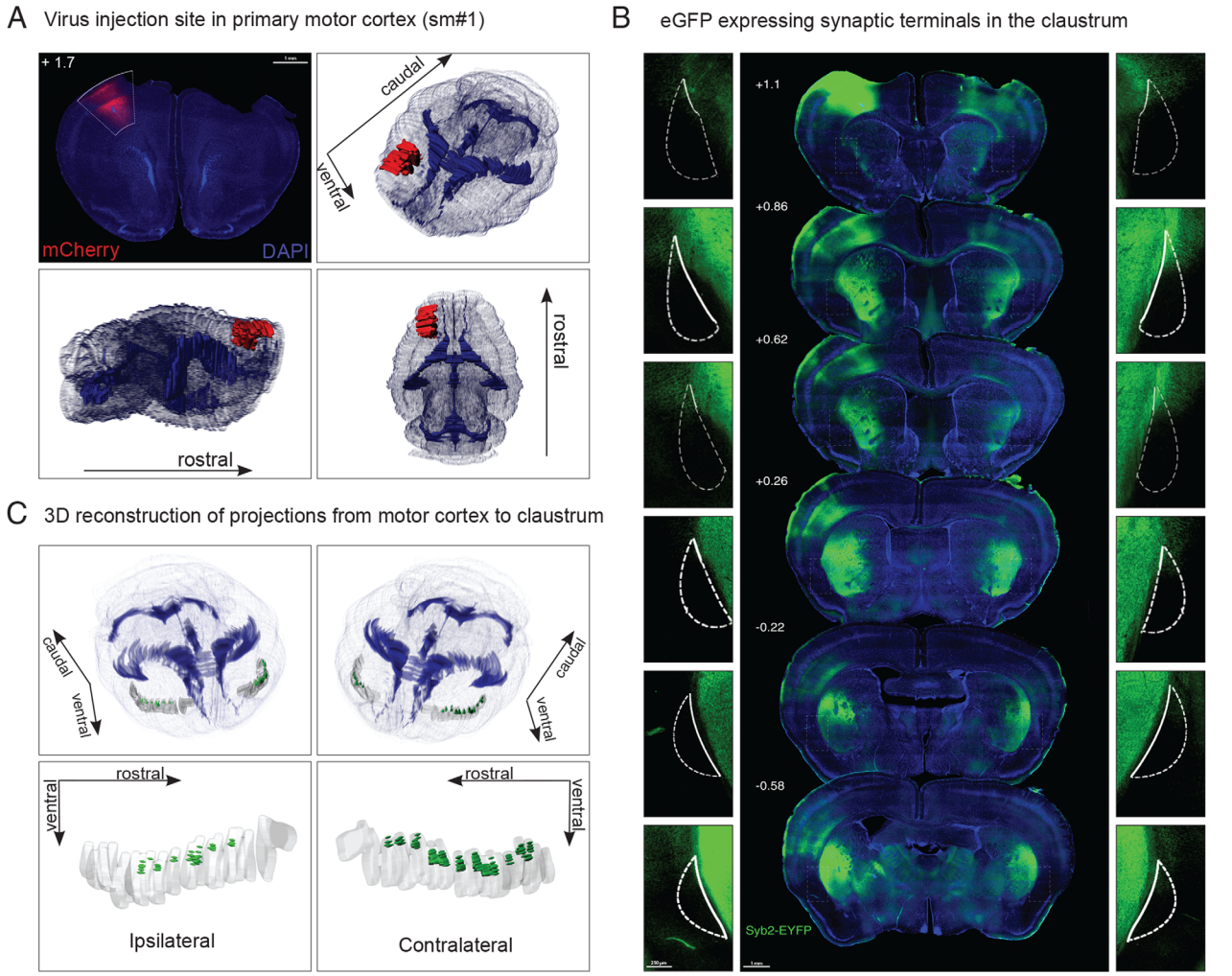

Figure 4. Projections from the primary motor cortex to the claustrum. (**A**) Top left: coronal section corresponding to the AAV-SynaptoTag injection site in the primary motor cortex of mouse Sm#1; DAPI nuclear staining is shown in blue; mCherry expression in red. Number indicates distance from Bregma in mm. Bottom left: reconstructed 3D view of the spread of the infection, as seen from the side. Bottom right: injection site as seen from above. Top right: angular view of the injection site. (**B**) Representative brain sections in rostrocaudal order. Middle: whole section images of motor cortical projections following immunostaining against eGFP. Numbers indicate distance from Bregma in mm. Side panels: ipsilateral (left) and contralateral (right) claustrum. (**C**) 3D reconstruction of the target region in the claustrum. Top left and right panels: angular view of the whole brain and overlay of the ipsilateral and contralateral claustri, respectively. Bottom left: reconstructed fluorescent signal in the ipsilateral claustrum. Bottom right: reconstructed fluorescent signal in the contralateral claustrum. The gray background is the outline of the reconstructed claustrum.

around the needle tract, in motor and prelimbic cortices. In mouse OI#2 the injection was centered in the lateral anterior olfactory cortex, and included some infected cells in the lateral piriform cortex. In both mice we found fluorescent signals in the amygdaloid complexes, the olfactory tubercle, the endopiriform nucleus, and the piriform cortex, all known targets of the olfactory system (Brunjes et al., 2005; Hintiryan et al., 2012).

Labeled terminals were found in the ventralmost segment of the claustrum of both mice, indicating that this region receives inputs from olfactory structures. The signal originating from olfactory neurons was found in the claustrum of mouse OI#1 in both hemispheres, but was visibly more prominent in the claustrum ipsilateral to the injection site.

In mouse OI#2 (rostral olfactory cortex) fluorescent terminals were found nearly exclusively on the side ipsilateral to the injection. A few labeled terminals were found in the contralateral claustrum at its caudal end. Inputs were denser at the ventral end of the claustrum (Fig. 7). While in principle a portion of the signal in mouse OI#1 could originate from a very small prefrontal contamination, the fact that injections in both the

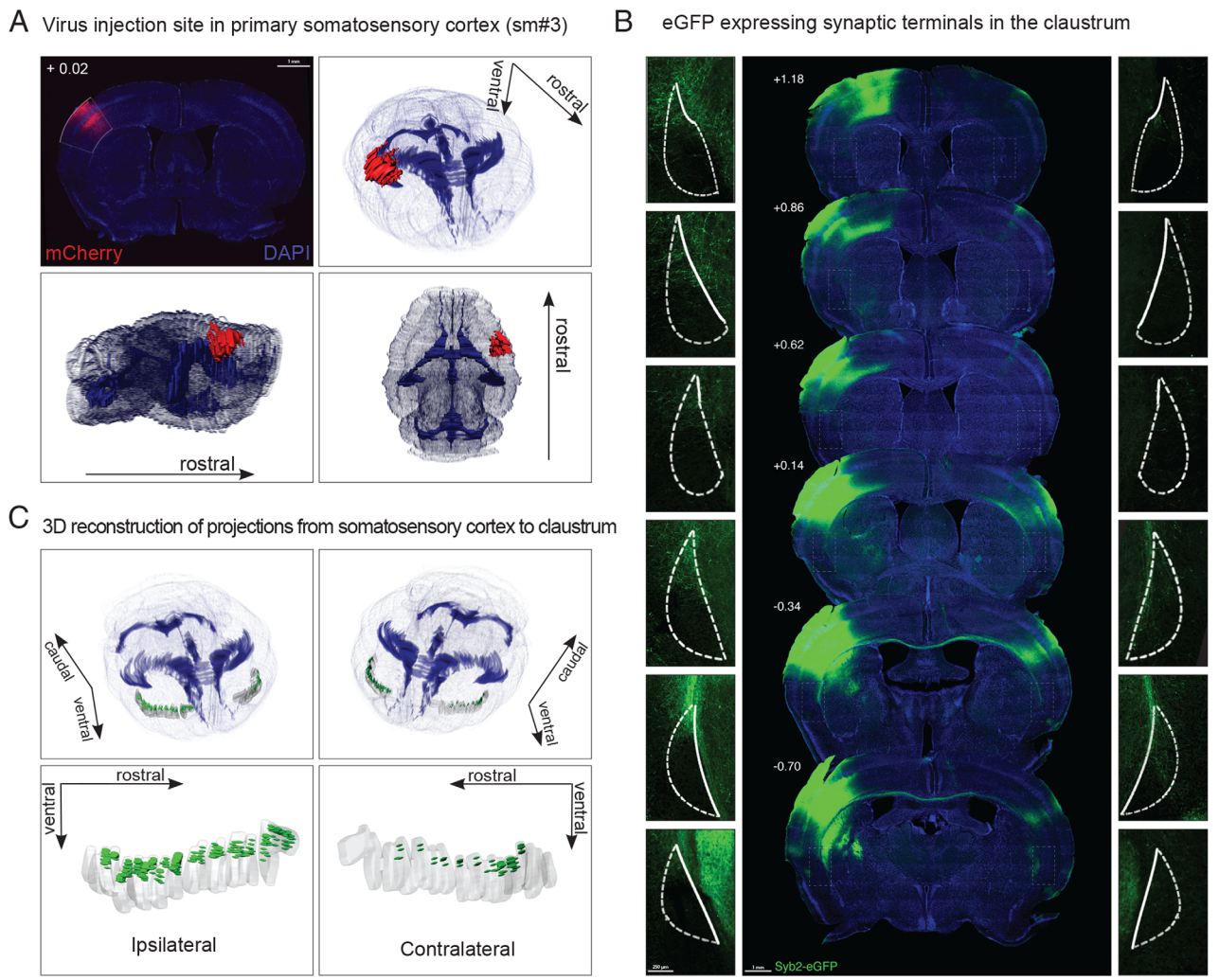

Figure 5. Projections from the somatosensory cortex to the claustrum. (**A**) Top left: coronal section corresponding to the AAV-SynaptoTag injection site in the somatosensory cortex of mouse Sm#3; DAPI nuclear staining is shown in blue; mCherry expression in red. Number indicates distance from Bregma in mm. Bottom left: reconstructed 3D view of the spread of the infection, as seen from the side. Bottom right: injection site as seen from above. Top right: angular view of the injection site. (**B**) Representative brain sections in rostrocaudal order. Middle: whole section images of somatosensory cortical projections following immunostaining against eGFP. Numbers indicate distance from Bregma in mm. Side panels: ipsilateral (left) and contralateral (right) claustrum. All the images were treated with the same brightness/contrast masks. Due to proximity to injection site, brightness adjustments reached saturation, causing reduced visibility of the claustrum signal. (**C**) 3D reconstruction of the target region in the claustrum. Top left and right panels: angular view of the whole brain and overlay of the ipsilateral and contralateral claustri, respectively. Bottom left: reconstructed fluorescent signal in the ipsilateral claustrum. Bottom right: reconstructed fluorescent signal in the contralateral claustrum. The gray background is the outline of the reconstructed claustrum.

olfactory bulb and the rostral olfactory cortex provide similar results, enhance confidence in the observation.

Prefrontal projections to the claustrum

In order to address the input from prefrontal cortical regions, we targeted the anterior cingulate cortex and orbitofrontal cortex in five mice (Figs. 8, 9). The anterior cingulate was targeted in mice Fr#1 and Fr#2. The orbitofrontal cortex was targeted in mice Fr#3, Fr#4, and Fr#5, at the intersection between the lateral and ventral orbitofrontal cortex (LO/VO).

Anterior cingulate

Both mice Fr#1 and Fr#2 expressed prominent infection throughout the anterior cingulate cortex (ACC). Labeled terminals were found in the retrosplenial cortex and the dorsal striatum, known targets of the ACC (Zingg et al., 2014; Guo et al., 2015). The fluorescent signal originating from ACC neurons was more prominent in contralateral, relative to the ipsilateral, claustrum. This was evident in mouse Fr#2, but was less obvious in mouse Fr#1 (Fig. 8). The distribution of the input to the claustrum appears not to be uniform along

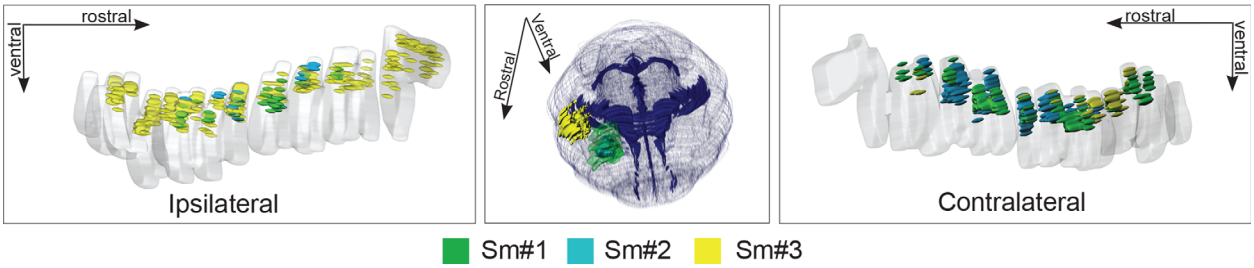

Figure 6. 3D superposition of all mice injected with AAV-SynaptoTag in the somatomotor areas. Different color hues refer to individual mice (Sm#1, Sm#2, Sm#3). according to the legend, enabling a comparison of individual injections and the fluorescence detected in the claustrum. Left: Reconstruction of the innervated region in the ipsilateral claustrum. Middle: Angular view of the spread of each infection in the site of origin. Right: Reconstruction of the innervated region in the contralateral claustrum.

the rostrocaudal axis, with more terminals found in the center of the claustrum, and sparser innervation toward the extremities. The ACC input to the claustrum targeted the majority of the claustrum along its dorsoventral axis, excluding the dorsalmost tip and not extending fully to the ventralmost aspect of the claustrum (Fig. 8).

Orbitofrontal

In mice Fr#3-5, the majority of infected cells were found in VO/LO, while a small number of infected cells were identified in the frontal association cortex or the anterior primary and secondary motor cortices. In all cases, labeled terminals were found in the dorsal striatum and the basolateral amygdala, as well as in primary motor cortex, known targets of the ventral orbitofrontal cortex (Zingg et al., 2014; Zimmermann et al., 2015). Orbitofrontal terminals in the claustrum were widespread and dense bilaterally, with a slight tendency to be more prominent in the ipsilateral claustrum (Fig. 9). In addition to covering the ventral claustrum, a signal was also present in the dorsal part of the claustrum, while a region in the center of the claustrum appeared excluded. Due to the infection spreading to a few cells in the primary and secondary motor cortex, it is possible that the motor cortex may be contributing part of the signal in the dorsal most tip of the claustrum.

In summary, we find heavy inputs from both orbitofrontal cortex (OFC) and ACC to the claustrum in all five prefrontal injections. The inputs to the claustrum from both these inputs are bilateral, albeit having different properties. ACC inputs are more limited to the ventral aspect of the claustrum, whereas the OFC inputs extend further dorsally. Moreover, while OFC inputs shun a region in the center of the claustrum, the ACC inputs appear to more heavily target this region. In this context, it is worth noting that there appears to be a trend towards mutual exclusion of ACC and OFC inputs, such that the middle section of the claustrum in the rostrocaudal aspect is targeted by ACC inputs, while the OFC input appears to preferentially innervate the rostral and caudal sections. This observation requires more direct experimental evidence, which is beyond the scope of the current study.

Orbitofrontal and auditory projections exclude an inhibitory "core" in the claustrum

While studying a number of projections to the claustrum, we observed that the input to claustrum appeared to form a "shell-like" structure, whereby fluorescence was denser in the perimeter of the claustrum, partially excluding the center of the claustrum in its mediolateral aspect. This is most apparent when viewing the auditory inputs to the claustrum (Fig. 3), as well as the olfactory inputs, which appear to "cup" the claustrum from its ventral aspect (Fig. 7), and the orbitofrontal inputs, which appear to create a thick "shell" in the perimeter of the claustrum (Fig. 9). To address this more rigorously, we utilized PV-CRE;Ai9 mice, in which parvalbumin-expressing interneurons (PV neurons) express a tdTomato transgene. Injection of the AAV-SynaptoTag virus to the orbitofrontal or auditory cortices of these mice revealed a clear structure of an inhibitory "core" of the claustrum, with a small number of positively labeled parvalbumin cell bodies, and a dense mesh of tdTomato-labeled neurites, surrounded by a eGFP-labeled "shell" comprised of inputs from the orbitofrontal and auditory cortices (Fig. 10).

DISCUSSION

In this study we investigated the organization of cortical inputs to the claustrum in mice, utilizing viral-based anterograde tracing of synaptic inputs, followed by image digitization and 3D reconstruction. The conclusions arising from our study are: 1) Inputs to the claustrum display a dorsoventral organization; 2) Inputs to the claustrum display a lateral preference, with visual, auditory and olfactory inputs projecting preferably ipsilaterally, while motor inputs project contralaterally, and

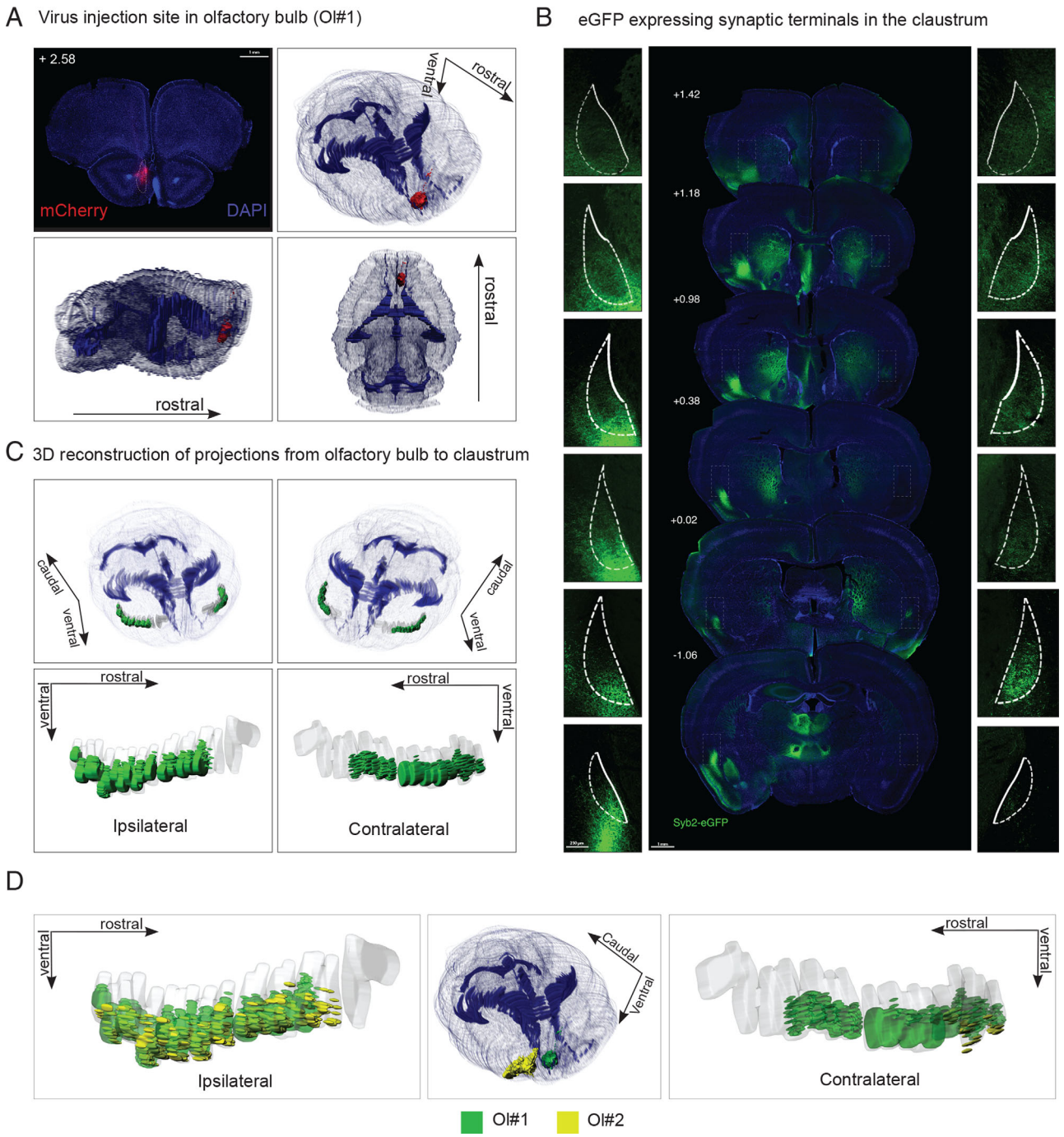

Figure 7. Projections from the olfactory bulb to the claustrum. (**A**) Top left: coronal section corresponding to the AAV-SynaptoTag injection site in the olfactory bulb of mouse OI#1; DAPI nuclear staining is shown in blue; mCherry expression in red. Number indicates distance from Bregma in mm. Bottom left: reconstructed 3D view of the spread of the infection, as seen from the side. Bottom right: injection site as seen from above. Top right: angular view of the injection site. (**B**) Representative brain sections in rostrocaudal order. Middle: whole section images of olfactory cortical projections following immunostaining against eGFP. Numbers indicate distance from Bregma in mm. Side panels: ipsilateral (left) and contralateral (right) claustrum. (**C**) 3D reconstruction of the target region in the claustrum. Top left and right panels: angular view of the whole brain and overlay of the ipsilateral and contralateral claustri, respectively. Bottom left: reconstructed fluorescent signal in the ipsilateral claustrum. Bottom right: reconstructed fluorescent signal in the contralateral claustrum. The gray background is the outline of the reconstructed claustrum. **(D)** 3D superposition of both mice injected with AAV-SynaptoTag to olfactory regions (OI#1, OI#2). Different color hues refer to individual mice according to the legend, enabling a comparison of individual injections and their projection to the claustrum. Left: reconstruction of the innervated region in the ipsilateral claustrum. Middle: angular view of the spread of each infection in the site of origin. Right: reconstruction of the innervated region in the contralateral claustrum.

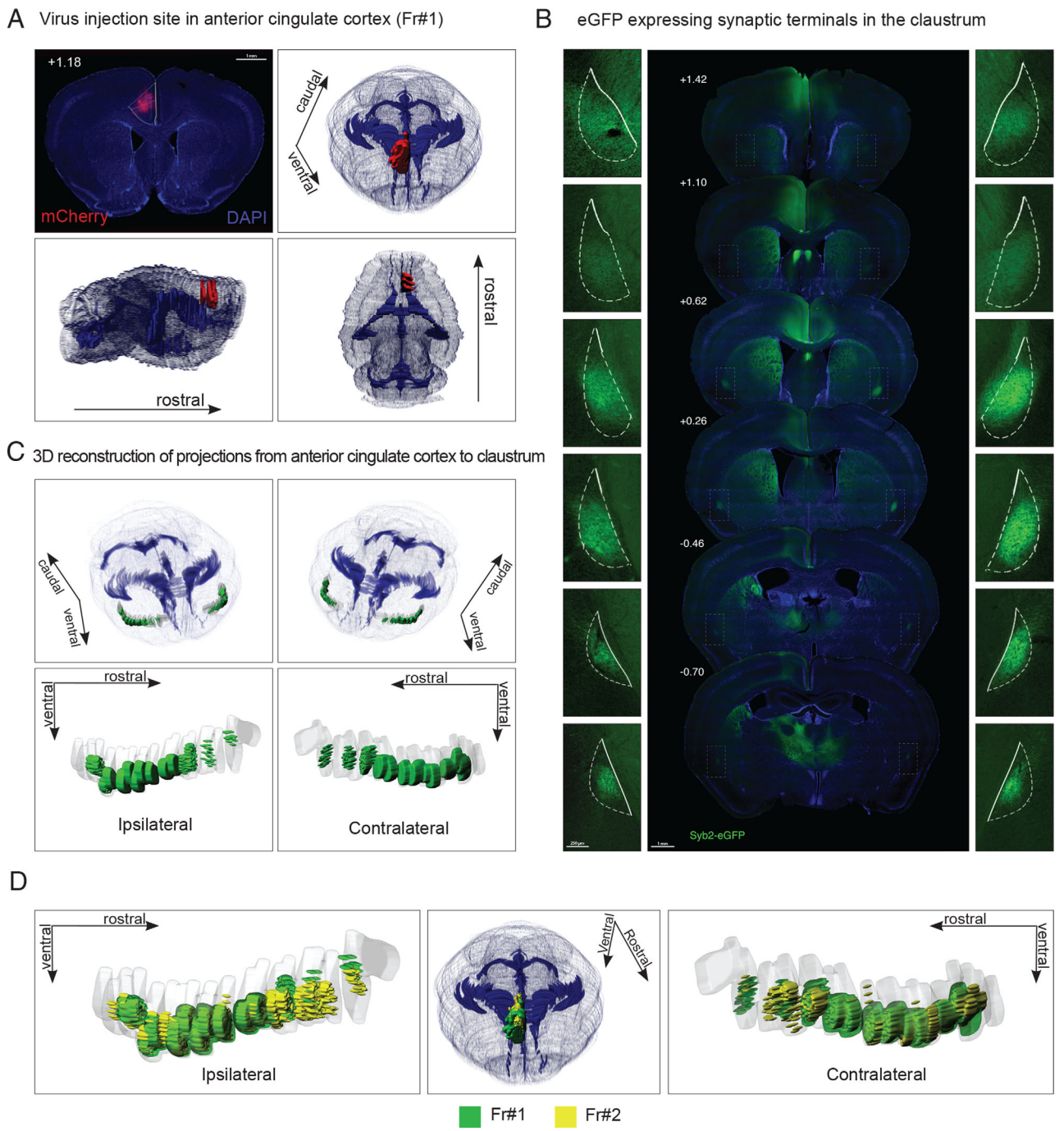

Figure 8. Projections from the anterior cingulate cortex to the claustrum. (**A**) Top left: coronal section corresponding to the AAV-SynaptoTag injection site in the anterior cingulate cortex of mouse Fr#1; DAPI nuclear staining is shown in blue; mCherry expression in red. Number indicates distance from Bregma in mm. Bottom left: reconstructed 3D view of the spread of the infection, as seen from the side. Bottom right: injection site as seen from above. Top right: angular view of the injection site. (**B**) Representative brain sections in rostrocaudal order. Middle: whole section images of cingulate cortical projections following immunostaining against eGFP. Numbers indicate distance from Bregma in mm. Side panels: ipsilateral (left) and contralateral (right) claustrum. (**C**) 3D reconstruction of the target region in the claustrum. Top left and right panels: angular view of the whole brain and overlay of the ipsilateral and contralateral claustri, respectively. Bottom left: reconstructed fluorescent signal in the ipsilateral claustrum. Bottom right: reconstructed fluorescent signal in the contralateral claustrum. The gray background is the outline of the reconstructed claustrum. (**D**) 3D superposition of all mice injected with AAV-SynaptoTag to the anterior cingulate cortex (Fr#1, Fr#2). Different color hues refer to individual mice according to the legend, enabling a comparison of individual injections and their projection to the claustrum. Left: reconstruction of the innervated region in the ipsilateral claustrum. Middle: angular view of the spread of each infection in the site of origin. Right: reconstruction of the innervated region in the contralateral claustrum.

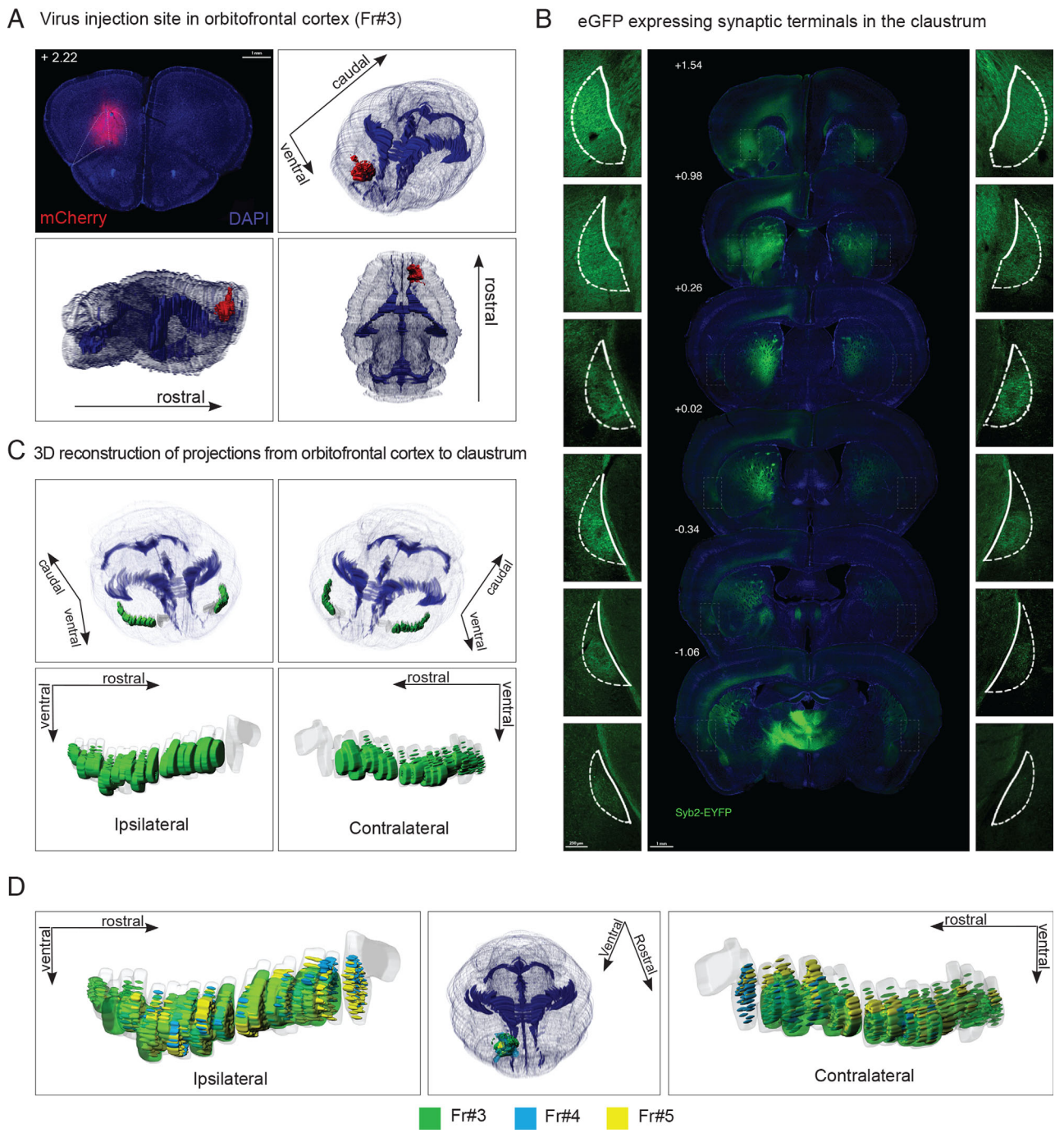

Figure 9. Projections from the orbitofrontal cortex to the claustrum. (**A**) Top left: coronal section corresponding to the AAV-SynaptoTag injection site in the orbitofrontal cortex of mouse Fr#3; DAPI nuclear staining is shown in blue; mCherry expression in red. Number indicates distance from Bregma in mm. Bottom left: reconstructed 3D view of the spread of the infection, as seen from the side. Bottom right: injection site as seen from above. Top right: angular view of the injection site. (**B**) Representative brain sections in rostrocaudal order. Middle: whole section images of orbitofrontal cortical projections following immunostaining against eGFP. Numbers indicate distance from Bregma in mm. Side panels: ipsilateral (left) and contralateral (right) claustrum. (**C**) 3D reconstruction of the target region in the claustrum. Top left and right panels: angular view of the whole brain and overlay of the ipsilateral and contralateral claustri, respectively. Bottom left: reconstructed fluorescent signal in the ipsilateral claustrum. Bottom right: reconstructed fluorescent signal in the contralateral claustrum. The gray background is the outline of the reconstructed claustrum. The two most rostral sections in this sample were missing and therefore not digitized. (**D**) 3D superposition of all mice injected with AAV-SynaptoTag to the oribitofrontal cortex (Fr#3, Fr#4, Fr#5). Different color hues refer to individual mice according to the legend, enabling a comparison of individual injections and their projection to the claustrum. Left: reconstruction of the innervated region in the ipsilateral claustrum. Middle: angular view of the spread of each infection in the site of origin. Right: reconstruction of the innervated region in the contralateral claustrum.

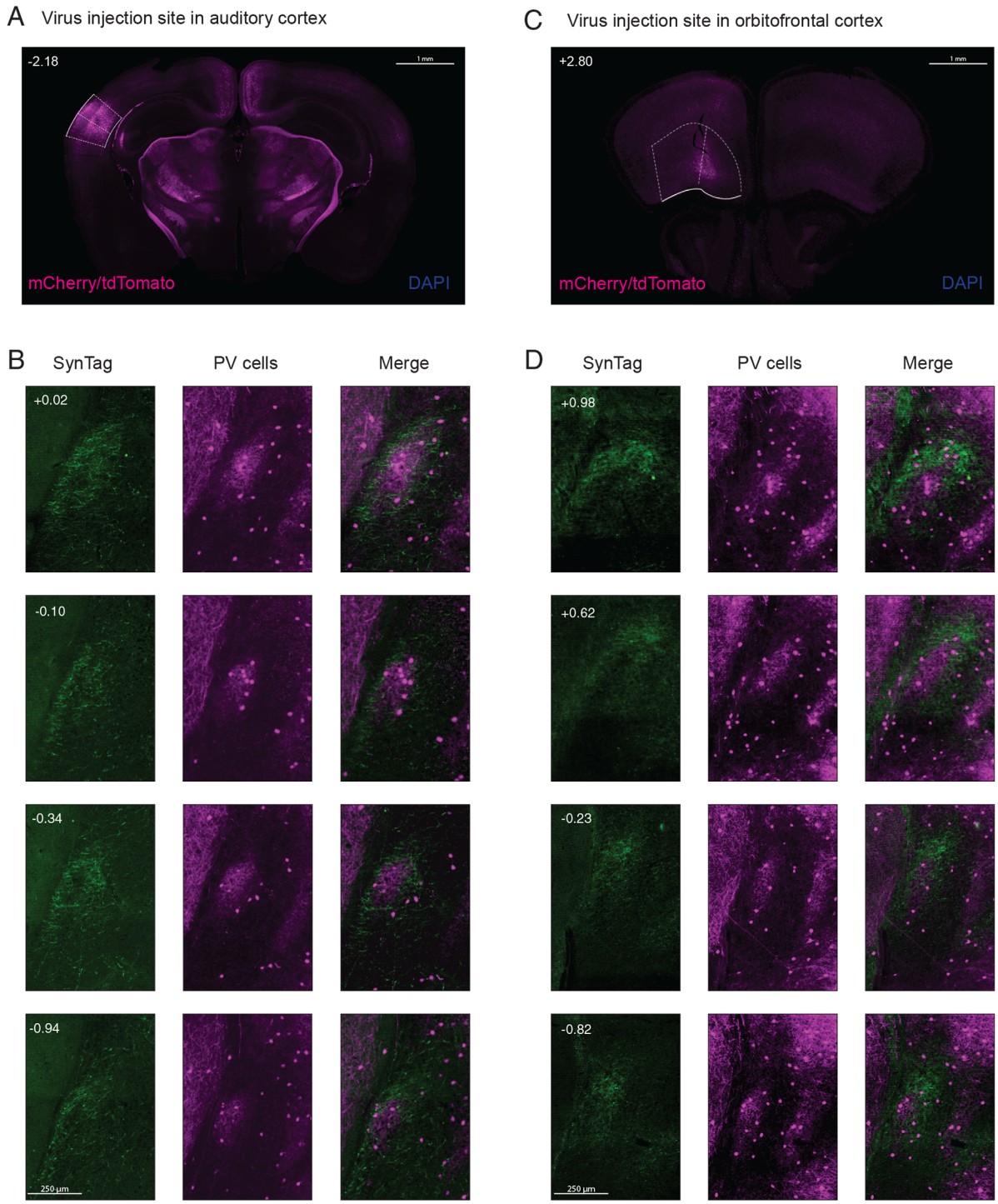

Figure 10. Core–shell organization in the claustrum. **(A)** Coronal section corresponding to the AAV-SynaptoTag injection site in the primary auditory cortex of a PV-Cre;Ai9 mouse. DAPI nuclear staining is shown in blue; mCherry expression in magenta shows the virus infection as well as PV labeled cells. Number indicates distance from Bregma in mm. **(B)** Image of the claustrum demonstrating a core–shell organization. Left: auditory innervation in the ipsilateral claustrum. Middle: PV expressing cells in the claustrum. Right: merged image. Number indicates distance from Bregma in mm. **(C)** Coronal section corresponding to the AAV-SynaptoTag injection site in the orbitofrontal cortex of PV-Cre;Ai9 mouse. DAPI nuclear staining is shown in blue; mCherry expression in magenta shows the virus infection as well as PV labeled cells. Number indicates distance from Bregma in mm. **(D)** Image of the claustrum demonstrating a core–shell organization. Left: orbitofrontal innervation in the ipsilateral claustrum. Middle: PV expressing cells in the claustrum. Right: merged image. Number indicates distance from Bregma in mm.

prefrontal inputs project almost equally to either hemisphere; 3) The inputs to the claustrum appear to demonstrate a core–shell structure, with some inputs to the claustrum preferentially innervating the periphery of the claustrum, while parvalbumin neurons create a dense mesh of neurites within a core region of the claustrum. This organization suggests the potential for a hierarchy of information processing within the claustrum, where internal and external layers may receive segregated inputs.

Dorsoventral organization with significant overlap

Overlaying the digitized representations of the cortical inputs to the claustrum demonstrates that one of the principles governing the organization of inputs to the claustrum is the predominance of a dorsoventral axis (Fig. 11). The dorsal tip of the claustrum receives somatosensory and motor information. More ventrally, the dorsal section of the claustrum receives auditory inputs, which also extend into the intermediate part of the claustrum. Visual input seems to be located in the central zone of the claustrum, extending ventrally, while the ventral end of the claustrum is innervated by olfactory inputs. Frontal projections, both from the ACC and the OFC, are more widespread, and overlap with most other sensory projections.

While there is a clear spatial segregation of inputs along the dorsoventral axis of the claustrum, we also observed significant overlap of inputs. For example, the visual input to the claustrum appears to be within a domain defined by the auditory inputs. More prominently, the prefrontal (OFC and ACC) inputs to the claustrum clearly overlap with the inputs from all the sensory modalities. This organization is consistent with a proposed role for prefrontal inputs in defining the rules of claustral communication with cortex, in the context of the "attentional hypothesis" for the function of the claustrum (Goll et al., 2015). Obviously, the coarse resolution of the current study does not provide conclusive evidence in favor of direct interactions between cortical inputs within the claustrum, which is best tested utilizing single-cell electrophysiological measurements. However, based on our observations we do have a strong expectation that prefrontal inputs will impact the majority of claustral neurons, regardless of the modality to which they respond.

Claustral connectivity of the mouse: a comparison with the rat and other species

Visual inputs to the claustrum have been studied in cats, monkeys, and rats (Sanides and Buchholtz, 1979; LeVay and Sherk, 1981b; Sherk and LeVay, 1981b; Grieve and Sillito, 1995; Smith and Alloway, 2014). In the cat, visual inputs were found in the dorsocaudal part of the ipsilateral claustrum (Sanides and Buchholtz, 1979), while in the rhesus monkey responses to visual stimulations were localized to the ventral portion of the claustrum (Remedios et al., 2010). There appears to be some variation in the extent of primary versus secondary visual inputs to the claustrum across species (Sherk, 1986). In the ferret, a clear hierarchy of input from the visual cortex to the claustrum was also observed, with lower visual areas providing very little input to the claustrum, while higher visual areas provided extensive input, which was widespread throughout the claustrum (Patzke et al., 2014). Sparse ipsilateral projections from V1 were also reported in the rat claustrum, as well as more prominent inputs from V2m (Smith and Alloway, 2014). Our results are consistent with these observations, as we observe limited ipsilateral inputs from primary visual cortex, while secondary visual cortex projects more widely (Fig. 2). It is important to note that the visual cortex of the mouse spans large cortical swaths and our injections cover only a portion of it for each injection. Potentially, the claustrum could be summing inputs from the whole visual cortex, such that projections from limited regions in visual cortex would only represent a small subset of the visual projections to the claustrum.

Auditory inputs to the claustrum have been studied in the cat, in which it has been described that inputs from all subdivisions of auditory cortex converge onto a restricted region in the claustrum. The inputs are predominantly ipsilateral and cover a large extent of the rostrocaudal axis, while concentrating in the center of the dorsoventral axis (Neal et al., 1986; Beneyto and Prieto, 2001). Our results also demonstrate a strong ipsilateral bias in the inputs from the auditory cortex; however, we observe a significant spread of the input within the ventral region of the claustrum (Fig. 3).

Somatosensory inputs to the claustrum have been reported in mice, cats, and monkeys. Cat S1 displays a somatotopic representation in the claustrum (Olson and Graybiel, 1980) and somatosensory inputs have been reported in mouse (Zingg et al., 2014) and monkey (Kunzle and Radtke-Schuller, 2001). The somatosensory system in rodents is an active sense. It requires active whisking or palpation in order to optimally acquire information from the environment. Therefore, the motor and sensory cortices can be viewed as a unified sensorimotor unit (Smith et al., 2012; Smith and Alloway, 2014). Rats and other nocturnal animals build up a representation of their surrounding world primarily through whisker-mediated somatosensation (Sofroniew and

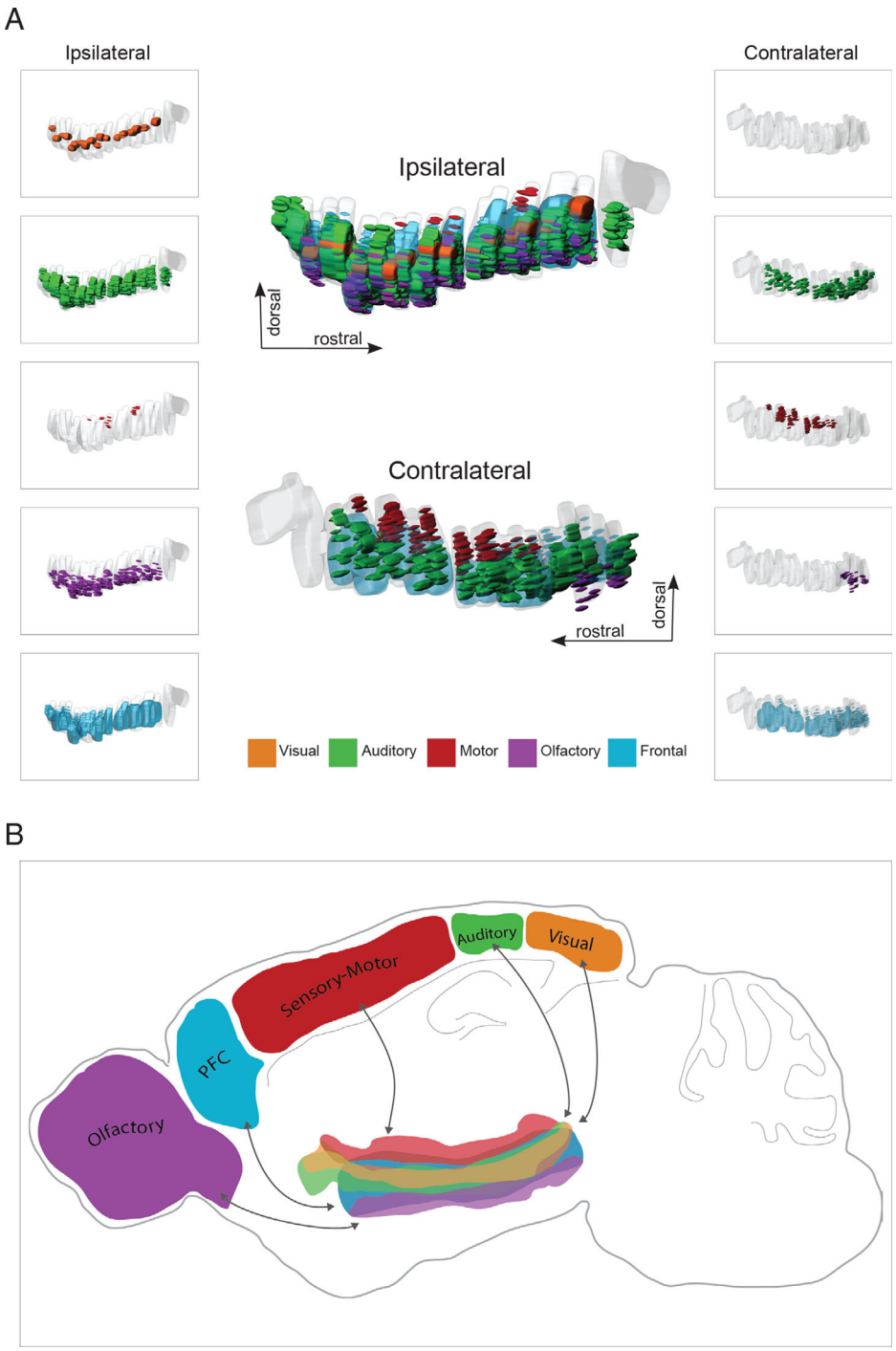

Figure 11. Summary of the cortical projections to the claustrum of the mouse. (**A**) Reconstructed claustral projections from visual (yellow; Vi#1), auditory (green; Au#1), somatomotor (red; Sm#2), olfactory (violet; Ol#2), and frontal (blue; Fr#3) cortical regions. The middle panels demonstrate the overlay of all the inputs within the claustrum (**B**) Cartoon image of the map of cortical projections onto the claustrum of the mouse.

Svoboda, 2015). Indeed, a significant projection to the claustrum has been described from the primary motor whisker region in rats, while inputs from the whisker region in the somatosensory cortex have not been found in rat (Alloway et al., 2009; Smith and Alloway, 2010; Smith et al., 2012), yet have been reported in mice (Zingg et al., 2014). However, neurons in the region of the claustrum that receives whisker motor innervations have been found to project back to the whisker motor cortex and the whisker somatosensory

cortex, demonstrating a cortico-claustral-cortical circuit (Alloway et al., 2009; Smith and Alloway, 2010; Smith et al., 2012; White et al., 2016). It has therefore been proposed that the claustrum functions in sensorimotor coordination of whisker movements necessary for orientation and object palpation (Smith et al., 2012; Sofroniew and Svoboda, 2015). The primary motor (MI) whisker region has been reported to project to the claustrum in both hemispheres, with denser projections to the contralateral claustrum (Alloway et al., 2009). Our results are overall consistent with the notion of somatomotor loops involving the claustrum, and recapitulate the observation of somatosensory and motor inputs to the claustrum (Figs. 4–6).

Very little work has been performed on inputs to the claustrum relating to the senses of taste or smell. As part of a multimodal investigation of the claustrum, neurons in the claustrum of the cat were found to respond to stimulation of the ipsilateral olfactory bulb (Segundo and Machne, 1956; Spector et al., 1974), and a tracing study has raised the possibility that the ventral segment of the cat claustrum receives olfactory input (Witter et al., 1988). These results have not gained significant attention, potentially due to the proximity of the claustrum to the piriform cortex and the endopiriform nucleus, which are associated with gustatory and olfactory processing. Furthermore, the endopiriform nucleus, located ventrally to the claustrum, has been shown to be connected with olfactory areas and has been hypothesized to be an olfactory structure, perhaps functioning as an "olfactory claustrum" (Witter et al., 1988; Behan and Haberly, 1999; Goll et al., 2015). Our results demonstrate that while the endopiriform nucleus indeed receives vast olfactory inputs, the claustrum is also innervated throughout its ventral half (Fig. 7). The identification of olfactory projections to the claustrum in mice is of potential significance for informing models regarding the function of the claustrum, especially considering the relative importance of olfactory information for the mouse.

A relatively large number of studies have addressed the prominent interaction between the claustrum and higher frontal and association regions in rat, cat, monkey, and humans (Divac et al., 1978; LeVay and Sherk, 1981b; Pearson et al., 1982; Markowitsch et al., 1984; Sloniewski et al., 1986; Witter et al., 1988; Clasca et al., 1992; Tanne-Gariepy et al., 2002; Vertes, 2004; Hur and Zaborszky, 2005; Hoover and Vertes, 2007; Mathur et al., 2009; Smith and Alloway, 2010, 2014; Reser et al., 2014; Sherk, 2014; Torgerson et al., 2015; White et al., 2016). Retrograde tracing in rats has demonstrated that claustral neurons projecting to the ACC are densely packed and distributed evenly throughout the claustrum (White et al., 2016). It should be noted that our injections covered extensive regions within the ACC, and may mask more subtle dorsoventral organization of the inputs from ACC / frontal eye field, as described in the rat (Brecht et al., 2004; Smith et al., 2012; Smith and Alloway, 2014). In the cat, retrograde tracer injections to the dorsal claustrum resulted in labeling of neurons in the orbitofrontal cortex (Witter et al., 1988), while anterograde labeling experiments in rodents demonstrated a prominent bilateral input to the claustrum from the ACC and infralimbic cortex (Smith and Alloway, 2014; Zingg et al., 2014; White et al., 2016). Our results are consistent with previous observations, as we observe heavy bilateral inputs to the claustrum from both the ACC and the OFC. Interestingly, our results suggest that the ACC and OFC impact mutually exclusive regions in the claustrum, with the ACC input preferentially targeting the center of the claustrum in both its rostrocaudal and dorsoventral axes, while the OFC input appears to prefer the formation of a "shell" around this potential "core." This observation suggests that these two major frontal association regions may impact different domains in the claustrum, raising the notion that within the small structure of the claustrum multiple functional domains may exist.

Additional organizational principles governing cortical inputs to the claustrum?

In the coronal sections shown in this study, some cortical projections appear to avoid a central aspect of the claustrum, defining a potential "shell" vs. "core" structure for the claustrum. This organization appears to be the case for olfactory inputs, which "cup" the claustrum from its ventral aspect, as well as the input from auditory cortex and orbitofrontal cortex, both of which are found to exclude the central portion of the claustrum. In contrast, the visual cortical inputs to the claustrum appeared to cluster in the center of the claustrum, and the somatomotor inputs invade the dorsal part of the claustrum with no apparent avoidance of defined territories within the claustrum.

A core–shell organization has been previously proposed for the claustrum (Real et al., 2003; Davila et al., 2005; Hinova-Palova et al., 2007; Rahman and Baizer, 2007; Pirone et al., 2014). This organization has been proposed primarily based on observations that inhibitory interneurons expressing parvalbumin and calretinin were found to be preferentially localized in the central and ventral region of the dorsal claustrum, while a dense plexus of axons form a shell around this core. In addition, cortical projecting neurons were labeled in a dorsal–shell-like region (LeVay and Sherk, 1981b). Our

results are consistent with the notion that the claustrum exhibits an internal structure, potentially defining a hierarchy of connectivity and information processing. Furthermore, long-range intra-claustral connections have been reported (Behan and Haberly, 1999; Zhang et al., 2001; Smith and Alloway, 2010) and the cell bodies and dendrites of interneurons appear to be preferentially oriented along the rostrocaudal axis, consistent with a potential function in communicating between the regions of the claustrum (Rahman and Baizer, 2007). Recent electrophysiological observations demonstrate a laminar structure of the claustrum (Orman, 2015), with the conclusion that the claustrum has strong excitatory connections organized along its rostrocaudal axis, with little connectivity between claustral excitatory neurons along the dorsoventral axis. A recent detailed patch-clamp study of connectivity in the claustrum in coronal sections of the mouse brain described prevalent inhibitory connectivity of PV neurons onto claustral neurons, and prevalent feedforward inhibition driven by cortical inputs to the claustrum (Kim et al., 2016). Virtually no connections were observed between excitatory claustral neurons in this study, potentially consistent with the observation of Orman (2015), as these connections were investigated in coronal slices, potentially destroying lateral connectivity in the claustrum.

It should be noted that the concept of a core–shell structure for the claustrum has been contended, with the suggestion that the "shell" may represent layer VI neurons of the insular cortex (Mathur et al., 2009; Mathur, 2014). This raises a more general issue, regarding the anatomical definition of the claustrum. Mathur and colleagues (Mathur et al., 2009; Mathur, 2014; White et al., 2016) have proposed that the claustrum can be defined based on expression of the gene GNG2 and exclusion of the gene CRYM. As they observe that the domain of GNG2 expression correlates with a region of dense labeling for parvalbumin (PV), they suggest that PV expression may be utilized to identify the boundaries of the claustrum. Here we propose that the definition of the claustrum in the mouse extends beyond the PV-rich domain. Consistent with this reasoning, GNG2 expression in the mouse (as demonstrated in the Allen Mouse Brain Atlas) encompasses the region we define as claustrum in the current study (core and shell), and appears to even extend further both dorsally and laterally. Alternatively, the apparent discrepancy may be due to anatomical differences between rat and mice, as well as increased sensitivity of antibody staining for PV in comparison to native fluorescence of transgenically expressed tdTomato in the PV-CRE;Ai9 mice.

An additional issue relating to the anatomical definitions of the claustrum is that it has been contested whether rostral coronal sections of the rat brain, in which the striatum is not found, should be regarded as claustrum (Mathur, 2009). This prestriatal region is much smaller in the mouse, and our analysis included only one such section, which we deemed claustral, as the signal observed within it appeared continuous with proceeding sections.

A universal strategy for connectomics: technical considerations

Beyond providing a comprehensive study of cortical inputs to the claustrum, our study establishes a broadly applicable approach to reveal the organization of synaptic inputs to a defined brain structure. For example, it is clear that a map of the cortical projections to the dorsal striatum could be constructed based on reanalysis of the images presented in Figures 2–9, demonstrating a well-defined compartmentalization of inputs to the striatum along the dorsoventral and mediolateral axes. This type of analysis could, for example, direct the investigation of sensory integration in the striatum (Reig and Silberberg, 2014).

The advantages of the strategy we implemented in this study are largely based on the utilization of a virus expressing a protein-based synaptic marker. This marker (eGPF-Syb2) marks synaptic terminals, in contrast to a diffusible marker, which labels axons as they pass through a tissue. Furthermore, the synaptic signal can be amplified with antibody staining, providing additional sensitivity. The enhanced signal obtained utilizing our strategy may account for the identification of inputs to the claustrum, which previously may have been missed, as in the case of the somatosensory inputs to the dorsal claustrum and the ventral olfactory inputs, as well as the intensity of the visual inputs. This strategy could be even further enhanced by targeting genetically defined neuronal populations in mice, utilizing a CRE-dependent variant of the SynaptoTag construct (not described in this study).

The registration and digitization of the synaptic signal, defining 3D coordinates for each puncta, provides the opportunity for comparison across individuals by overlaying data obtained from multiple subjects. This enables a direct comparison of experimental repetitions, as well as comparison of the domain targeted by different projections. Once implemented in a 3D visualization platform, the digitized data are easily viewed from different perspectives, enabling additional insight into the spatial organization of the results. A universally accepted coordinate system onto which such data are registered could provide a platform for collaboration and resolving ambiguities. A number of efforts are being

developed along these lines, including the Allen Mouse Brain Atlas (http://mouse.brain-map.org), Mouse Connectome Project (http://www.mouseconnectome.org), and the Waxholm Space Atlas. However, they do not, as of yet, provide an accessible tool for registration of data obtained by independent investigators, the need for which is likely to increase as the field of connectomics matures.

It is important to note that the method we applied in this study is not free from fault. The digitization approach we implemented is aimed at providing a binary representation of the location of the projection within the claustrum, and therefore does not provide a relative measure of the intensity of the projection to the claustrum. In addition, the digitization, as performed, results in a reduction in the spatial resolution compared to the raw images. These two caveats are common to most strategies for representation of tracing in contemporary studies. In future developments of this approach, we plan to implement a semiautomated pipeline, enhancing the information content of the data both with relation to intensity and resolution, as well as reducing the effort invested in image digitization.

Perspective: from anatomy to function?

The claustrum, with its high connectivity, has created a high level of intrigue regarding its function, and a number of compelling theories have been suggested. These have developed from proposing that the claustrum functions as a relay station (Olson and Graybiel, 1980; LeVay and Sherk, 1981b; Sherk and LeVay, 1983), potentially binding information across modalities (Pearson et al., 1982; Ettlinger and Wilson, 1990), to supporting consciousness (Crick and Koch, 2005). More recent theories suggest a function for the claustrum in coordinating cortical activity (Alloway et al., 2009; Mathur et al., 2009; Remedios et al., 2010; Smith and Alloway, 2010; Smith et al., 2012; Mathur, 2014; Remedios et al., 2014; Reser et al., 2014; Smith and Alloway, 2014; Smythies et al., 2014; Goll et al., 2015). Major questions still remain open, such as the question of whether the claustrum is an integrator of information or, alternatively, consists of segregated functional units (Remedios et al., 2010; Smith et al., 2012; Baizer et al., 2014; Sherk, 2014). Our observations are suggestive of an overall segregation of inputs within the claustrum, with somatomotor inputs invading the dorsal end of the claustrum, and olfactory inputs invading the ventral end, while auditory inputs appear to create a "shell" around a PV-expressing inhibitory "core." Visual inputs focus within a central domain in the claustrum, and may also be localized to this "core," but this has not been directly investigated. Frontal inputs also appear to segregate, with ACC inputs appearing to target the "core" region (see also White et al., 2016), while OFC inputs may target the "shell." The overlap of the frontal inputs with the sensory inputs to the claustrum (ACC with visual; OFC with auditory, olfactory, and somatomotor) is suggestive of a hierarchical organization, whereby the frontal inputs interact with inputs from the sensory modalities (as also proposed by White et al., 2016). Viewed from the perspective of the "attentional hypothesis" for the function of the claustrum (Mathur, 2014; Goll et al., 2015), this overlapping connectivity is consistent with a potential role for the frontal inputs in modulating the representation of the sensory inputs within the claustrum, as a mechanism for implementing a defined "attentional strategy." Thus, our study poses testable hypotheses, which will have to be answered on the way to resolving the function of the claustrum.

ACKNOWLEDGMENTS

We thank Dr. Wei Xu for the gift of the AAV-mCherry-IRES-eGFP-Syb2 viral construct. We thank Dr. Naomi Book-Melamed, head of the microscopy unit at the Life Science Institute for technical support and access to software. We appreciate the gift of PV-Cre;Ai9 mice from Prof. Adi Mizrahi. We also thank the members of the Citri lab for support and helpful discussions. The contribution of Drs. Inbal Goshen and Alon Zaslaver to the final format of the text is appreciated.

CONFLICT OF INTEREST

The authors declare no conflicts of interest.

ROLE OF AUTHORS

All authors had full access to all the data in the study and take responsibility for the integrity of the data and the accuracy of the data analysis. Study concept and design: GA, AN, NR, AC. Virus preparation: MG. Surgery and Virus injections: GA, AN. Acquisition of data: GA, AN, NR. Analysis and interpretation of data: GA, AN, NR. Drafting of the manuscript: GA, AN, NR, AC. Obtained funding: AC. Study supervision: AC.

LITERATURE CITED

Alloway KD, Smith JB, Beauchemin KJ, Olson ML. 2009. Bilateral projections from rat MI whisker cortex to the neostriatum, thalamus, and claustrum: forebrain circuits for modulating whisking behavior. J Comp Neurol 515: 548–564.

Baizer JS, Sherwood CC, Noonan M, Hof PR. 2014. Comparative organization of the claustrum: what does structure tell us about function? Front Syst Neurosci 8:117.

Behan M, Haberly LB. 1999. Intrinsic and efferent connections of the endopiriform nucleus in rat. J Comp Neurol 408: 532–548.

Beier KT, Saunders AB, Oldenburg IA, Sabatini BL, Cepko CL. 2013. Vesicular stomatitis virus with the rabies virus glycoprotein directs retrograde transsynaptic transport among neurons in vivo. Front Neural Circuits 7:11.

Beneyto M, Prieto JJ. 2001. Connections of the auditory cortex with the claustrum and the endopiriform nucleus in the cat. Brain Res Bull 54:485–498.

Brecht M, Krauss A, Muhammad S, Sinai-Esfahani L, Bellanca S, Margrie TW. 2004. Organization of rat vibrissa motor cortex and adjacent areas according to cytoarchitectonics, microstimulation, and intracellular stimulation of identified cells. J Comp Neurol 479:360–373.

Brunjes PC, Illig KR, Meyer EA. 2005. A field guide to the anterior olfactory nucleus (cortex). Brain Res Brain Res Rev 50:305–335.

Carey RG, Neal TL. 1985. The rat claustrum: afferent and efferent connections with visual cortex. Brain Res 329: 185–193.

Carey RG, Neal TL. 1986. Reciprocal connections between the claustrum and visual thalamus in the tree shrew (Tupaia glis). Brain Res 386:155–168.

Clarey JC, Irvine DR. 1986. Auditory response properties of neurons in the claustrum and putamen of the cat. Exp Brain Res 61:432–437.

Clasca F, Avendano C, Roman-Guindo A, Llamas A, Reinoso-Suarez F. 1992. Innervation from the claustrum of the frontal association and motor areas: axonal transport studies in the cat. J Comp Neurol 326:402–422.

Crick FC, Koch C. 2005. What is the function of the claustrum? Philos Trans R Soc Lond B Biol Sci 360:1271–1279.

Davila JC, Real MA, Olmos L, Legaz I, Medina L, Guirado S. 2005. Embryonic and postnatal development of GABA, calbindin, calretinin, and parvalbumin in the mouse claustral complex. J Comp Neurol 481:42–57.

Divac I, Kosmal A, Bjorklund A, Lindvall O. 1978. Subcortical projections to the prefrontal cortex in the rat as revealed by the horseradish peroxidase technique. Neuroscience 3:785–796.

Druga R. 2014. The structure and connections of the claustrum. In: Smythies JR, Edelstein LR, Ramachandran VS, editors. The claustrum. San Diego: Academic Press. p 29–84.

Ettlinger G, Wilson WA. 1990. Cross-modal performance: behavioural processes, phylogenetic considerations and neural mechanisms. Behav Brain Res 40:169–192.

Goll Y, Atlan G, Citri A. 2015. Attention: the claustrum. Trends Neurosci 38:486–495.

Grieve KL, Sillito AM. 1995. Differential properties of cells in the feline primary visual cortex providing the corticofugal feedback to the lateral geniculate nucleus and visual claustrum. J Neurosci 15:4868–4874.

Guo Q, Wang D, He X, Feng Q, Lin R, Xu F, Fu L, Luo M. 2015. Whole-brain mapping of inputs to projection neurons and cholinergic interneurons in the dorsal striatum. PLoS One 10:e0123381.

Hinova-Palova DV, Edelstein LR, Paloff AM, Hristov S, Papantchev VG, Ovtscharoff WA. 2007. Parvalbumin in the cat claustrum: ultrastructure, distribution and functional implications. Acta Histochem 109:61–77.

Hintiryan H, Gou L, Zingg B, Yamashita S, Lyden HM, Song MY, Grewal AK, Zhang X, Toga AW, Dong HW. 2012. Comprehensive connectivity of the mouse main olfactory bulb: analysis and online digital atlas. Front Neuroanat 6:30.

Hoover WB, Vertes RP. 2007. Anatomical analysis of afferent projections to the medial prefrontal cortex in the rat. Brain Struct Funct 212:149–179.

Hur EE, Zaborszky L. 2005. Vglut2 afferents to the medial prefrontal and primary somatosensory cortices: a combined retrograde tracing in situ hybridization study. J Comp Neurol 483:351–373.

Khibnik LA, Tritsch NX, Sabatini BL. 2014. A direct projection from mouse primary visual cortex to dorsomedial striatum. PLoS One 9:e104501.

Kim J, Matney CJ, Roth RH, Brown SP. 2016. Synaptic organization of the neuronal circuits of the claustrum. J Neurosci 36:773–784.

Kowianski P, Morys J, Karwacki Z, Dziewiatkowski J, Narkiewicz O. 1998. The cortico-related zones of the rabbit claustrum—study of the claustrocortical connections based on the retrograde axonal transport of fluorescent tracers. Brain Res 784:199–209.

Kunzle H, Radtke-Schuller S. 2001. Cortical connections of the claustrum and subjacent cell groups in the hedgehog tenrec. Anat Embryol 203:403–415.

LeVay S. 1986. Synaptic organization of claustral and geniculate afferents to the visual cortex of the cat. J Neurosci 6:3564–3575.

LeVay S, Sherk H. 1981a. The visual claustrum of the cat. I. Structure and connections. J Neurosci 1:956–980.

LeVay S, Sherk H. 1981b. The visual claustrum of the cat. II. The visual field map. J Neurosci 1:981–992.

Li ZK, Takada M, Hattori T. 1986. Topographic organization and collateralization of claustrocortical projections in the rat. Brain Res Bull 17:529–532.

Macchi G, Bentivoglio M, Minciacchi D, Molinari M. 1981. The organization of the claustroneocortical projections in the cat studied by means of the HRP retrograde axonal transport. J Comp Neurol 195:681–695.

Macchi G, Bentivoglio M, Minciacchi D, Molinari M. 1983. Claustroneocortical projections studied in the cat by means of multiple retrograde fluorescent tracing. J Comp Neurol 215:121–134.

Madisen L, Zwingman TA, Sunkin SM, Oh SW, Zariwala HA, Gu H, Ng LL, Palmiter RD, Hawrylycz MJ, Jones AR, Lein ES, Zeng H. 2010. A robust and high-throughput Cre reporting and characterization system for the whole mouse brain. Nat Neurosci 13:133–140.

Markowitsch HJ, Irle E, Bang-Olsen R, Flindt-Egebak P. 1984. Claustral efferents to the cat's limbic cortex studied with retrograde and anterograde tracing techniques. Neuroscience 12:409–425.

Mathur BN. 2014. The claustrum in review. Front Syst Neurosci 8:48.

Mathur BN, Caprioli RM, Deutch AY. 2009. Proteomic analysis illuminates a novel structural definition of the claustrum and insula. Cereb Cortex 19:2372–2379.

McGeorge AJ, Faull RL. 1989. The organization of the projection from the cerebral cortex to the striatum in the rat. Neuroscience 29:503–537.

Milardi D, Bramanti P, Milazzo C, Finocchio G, Arrigo A, Santoro G, Trimarchi F, Quartarone A, Anastasi G, Gaeta M. 2015. Cortical and subcortical connections of the human claustrum revealed in vivo by constrained spherical deconvolution tractography. Cereb Cortex 25:406–414.

Minciacchi D, Molinari M, Bentivoglio M, Macchi G. 1985. The organization of the ipsi- and contralateral claustrocortical system in rat with notes on the bilateral claustrocortical projections in cat. Neuroscience 16:557–576.

Narkiewicz O. 1964. Degenerations in the claustrum after regional neocortical ablations in the cat. J Comp Neurol 123:335–355.

Neal JW, Pearson RC, Powell TP. 1986. The relationship between the auditory cortex and the claustrum in the cat. Brain Res 366:145–151.

Norita M. 1977. Demonstration of bilateral claustro-cortical connections in the cat with the method of retrograde

axonal transport of horseradish peroxidase. Arch Histol Japon Nihon Soshikigaku Kiroku 40:1–10.
Olson CR, Graybiel AM. 1980. Sensory maps in the claustrum of the cat. Nature 288:479–481.
Orman R. 2015. Claustrum: a case for directional, excitatory, intrinsic connectivity in the rat. J Physiol Sci 65:533–544.
Park S, Tyszka JM, Allman JM. 2012. The claustrum and insula in microcebus murinus: a high resolution diffusion imaging study. Front Neuroanat 6:21.
Patzke N, Innocenti GM, Manger PR. 2014. The claustrum of the ferret: afferent and efferent connections to lower and higher order visual cortical areas. Front Syst Neurosci 8:31.
Paxinos G, Franklin KBJ. 2013. Paxinos and Franklin's the mouse brain in stereotaxic coordinates. Amsterdam: Elsevier.
Pearson RC, Brodal P, Gatter KC, Powell TP. 1982. The organization of the connections between the cortex and the claustrum in the monkey. Brain Res 234:435–441.
Petrof I, Viaene AN, Sherman SM. 2015. Properties of the primary somatosensory cortex projection to the primary motor cortex in the mouse. J Neurophysiol 113:2400–2407.
Pirone A, Castagna M, Granato A, Peruffo A, Quilici F, Cavicchioli L, Piano I, Lenzi C, Cozzi B. 2014. Expression of calcium-binding proteins and selected neuropeptides in the human, chimpanzee, and crab-eating macaque claustrum. Front Syst Neurosci 8:99.
Pollak Dorocic I, Furth D, Xuan Y, Johansson Y, Pozzi L, Silberberg G, Carlen M, Meletis K. 2014. A whole-brain atlas of inputs to serotonergic neurons of the dorsal and median raphe nuclei. Neuron 83:663–678.
Rahman FE, Baizer JS. 2007. Neurochemically defined cell types in the claustrum of the cat. Brain Res 1159:94–111.
Real MA, Davila JC, Guirado S. 2003. Expression of calcium-binding proteins in the mouse claustrum. J Chem Neuroanat 25:151–160.
Reig R, Silberberg G. 2014. Multisensory integration in the mouse striatum. Neuron 83:1200–1212.
Remedios R, Logothetis NK, Kayser C. 2010. Unimodal responses prevail within the multisensory claustrum. J Neurosci 30:12902–12907.
Remedios R, Logothetis NK, Kayser C. 2014. A role of the claustrum in auditory scene analysis by reflecting sensory change. Front Syst Neurosci 8:44.
Reser DH, Richardson KE, Montibeller MO, Zhao S, Chan JM, Soares JG, Chaplin TA, Gattass R, Rosa MG. 2014. Claustrum projections to prefrontal cortex in the capuchin monkey (Cebus apella). Front Syst Neurosci 8:123.
Riche D, Lanoir J. 1978. Some claustro-cortical connections in the cat and baboon as studied by retrograde horseradish peroxidase transport. J Comp Neurol 177:435–444.
Sadowski M, Morys J, Jakubowska-Sadowska K, Narkiewicz O. 1997. Rat's claustrum shows two main cortico-related zones. Brain Res 756:147–152.
Sanides D, Buchholtz CS. 1979. Identification of the projection from the visual cortex to the claustrum by anterograde axonal transport in the cat. Exp Brain Res 34:197–200.
Segundo JP, Machne X. 1956. Unitary responses to afferent volleys in lenticular nucleus and claustrum. J Neurophysiol 19:325–339.
Sherk H. 1986. The claustrum and the cerebral cortex. In: Jones EG, Peters A, editors. Sensory-motor areas and aspects of cortical connectivity. Boston: Springer US. p 467–499.
Sherk H. 2014. Chapter 5. Physiology of the claustrum. In: Smythies JR, Edelstein LR, Ramachandran VS, editors. The claustrum. San Diego: Academic Press. p 177–191.
Sherk H, LeVay S. 1981a. The visual claustrum of the cat. III. Receptive field properties. J Neurosci 1:993–1002.
Sherk H, LeVay S. 1981b. Visual claustrum: topography and receptive field properties in the cat. Science 212:87–89.
Sherk H, LeVay S. 1983. Contribution of the cortico-claustral loop to receptive field properties in area 17 of the cat. J Neurosci 3:2121–2127.
Sloniewski P, Usunoff KG, Pilgrim C. 1986. Retrograde transport of fluorescent tracers reveals extensive ipsi- and contralateral claustrocortical connections in the rat. J Comp Neurol 246:467–477.
Smith JB, Alloway KD. 2010. Functional specificity of claustrum connections in the rat: interhemispheric communication between specific parts of motor cortex. J Neurosci 30: 16832–16844.
Smith JB, Alloway KD. 2014. Interhemispheric claustral circuits coordinate sensory and motor cortical areas that regulate exploratory behaviors. Front Syst Neurosci 8:93.
Smith JB, Radhakrishnan H, Alloway KD. 2012. Rat claustrum coordinates but does not integrate somatosensory and motor cortical information. J Neurosci 32:8583–8588.
Smythies J, Edelstein L, Ramachandran V. 2014. Hypotheses relating to the function of the claustrum II: does the claustrum use frequency codes? Front Integr Neurosci 8:7.
Sofroniew NJ, Svoboda K. 2015. Whisking. Curr Biol 25:R137–140.
Spector I, Hassmannova Y, Albe-Fessard D. 1970. A macrophysiological study of functional organization of the claustrum. Exp Neurol 29:31–51.
Spector I, Hassmannova J, Albe-Fessard D. 1974. Sensory properties of single neurons of cat's claustrum. Brain Res 66:39–65.
Tanne-Gariepy J, Boussaoud D, Rouiller EM. 2002. Projections of the claustrum to the primary motor, premotor, and prefrontal cortices in the macaque monkey. J Comp Neurol 454:140–157.
Torgerson CM, Irimia A, Goh SY, Van Horn JD. 2015. The DTI connectivity of the human claustrum. Hum Brain Mapp 36:827–838.
Vertes RP. 2004. Differential projections of the infralimbic and prelimbic cortex in the rat. Synapse 51:32–58.
White MG, Cody PA, Bubser M, Wang H-D, Deutch AY, Mathur BN. 2016. Cortical hierarchy governs rat claustrocortical circuit organization. J Comp Neurol doi: 10.1002/cne.23970.
Witter MP, Room P, Groenewegen HJ, Lohman AH. 1988. Reciprocal connections of the insular and piriform claustrum with limbic cortex: an anatomical study in the cat. Neuroscience 24:519–539.
Xu W, Sudhof TC. 2013. A neural circuit for memory specificity and generalization. Science 339:1290–1295.
Xu W, Morishita W, Buckmaster PS, Pang ZP, Malenka RC, Sudhof TC. 2012. Distinct neuronal coding schemes in memory revealed by selective erasure of fast synchronous synaptic transmission. Neuron 73:990–1001.
Zhang X, Hannesson DK, Saucier DM, Wallace AE, Howland J, Corcoran ME. 2001. Susceptibility to kindling and neuronal connections of the anterior claustrum. J Neurosci 21: 3674–3687.
Zhou J, Wen Y, She L, Sui YN, Liu L, Richards LJ, Poo MM. 2013. Axon position within the corpus callosum determines contralateral cortical projection. Proc Natl Acad Sci U S A 110:E2714–2723.
Zimmermann KS, Yamin JA, Rainnie DG, Ressler KJ, Gourley SL. 2015. Connections of the mouse orbitofrontal cortex and regulation of goal-directed action selection by BDNF-TrkB. Biol Psychiatry [Epub ahead of print].
Zingg B, Hintiryan H, Gou L, Song MY, Bay M, Bienkowski MS, Foster NN, Yamashita S, Bowman I, Toga AW, Dong HW. 2014. Neural networks of the mouse neocortex. Cell 156:1096–1111.